Development and Capabilities of the NASA Flight Dynamics Research Facility

C. Michael Fremaux,* Benjamin M. Simmons,† and D. Bruce Owens‡
NASA Langley Research Center, Hampton, Virginia 23681

Dan D. Vicroy§
Adaptive Aerospace Group, Inc., Hampton, Virginia 23666

David B. Storch¶
NASA Langley Research Center, Hampton, Virginia 23681

The Flight Dynamics Research Facility (FDRF) is the first major wind tunnel built by NASA in over forty years. FDRF is a large, subsonic tunnel with a vertical test section for conducting all manner of flight dynamics research from basic stability and controllability to free-fall dynamic stability and aircraft spin and spin-recovery testing. When it becomes operational in the summer of 2025, it will replace the current Langley 20-Foot Vertical Spin Tunnel and 12-Foot Low-Speed Tunnel. This paper documents a brief history of the current flight-dynamics testing facilities, the development of the FDRF concept, tunnel performance requirements, planned research capabilities, tests to baseline performance, current construction status, and projected completion schedule.

I. Introduction

The Flight Dynamics Research Facility (FDRF) is the first major wind tunnel built by NASA since the opening of the National Transonic Facility (NTF) in the early 1980s. FDRF is a large, subsonic tunnel with a vertical test section for conducting all manner of flight dynamics research, from basic stability and controllability, to atmospheric entry vehicle free-fall dynamic stability, and aircraft spin and spin-recovery characterization. The FDRF project had a decades-long genesis in terms of multiple internal studies preceding it, beginning in the mid-1990s. The project itself gained traction in the mid-2010s as will be discussed in more detail in the next section. When it becomes operational in the summer of 2025, it will replace the current Langley 20-Foot Vertical Spin Tunnel and 12-Foot Low-Speed Tunnel, each of which has been operating continually for over eighty years. This paper will document a brief history of the current flight-dynamics testing facilities, the development of the FDRF concept, tunnel performance requirements, planned research capabilities, tests to baseline performance, current construction status, and projected completion schedule.

II. Background, Historical Perspective, and Legacy Facilities

Experimental testing of vehicle stability characteristics in specialized wind tunnels has a long and productive history at NASA Langley Research Center (LaRC), dating to the early 1930s [1–3] when the center was known as the National Advisory Committee for Aeronautics (NACA) Langley Memorial Aeronautical Laboratory. Photos of the earliest flight-dynamics specialty tunnels are shown in Figs. 1-5. Currently, LaRC has two tunnels focused on flight dynamics testing: The 12-Foot Low-Speed Tunnel (12-Foot) and the 20-Foot Vertical Spin Tunnel (VST) [3]. These tunnels have been in continual operation since 1939 for 12-Foot and 1941 for VST. A contemporary photo of the two tunnels, along with their adjacent support buildings, is shown in Fig. 6.

12-Foot was originally developed as a free-flight tunnel for testing the stability and controllability of small, dynamically-scaled models [4]. Using a hydraulically-actuated tilting test section that could be adjusted in pitch on-the-fly to match the glide slope of an unpowered model, multiple pilots (roll/yaw, test section pitch angle, and

*Chief Engineer for Intelligent Flight Systems, Research Directorate, Associate Fellow AIAA.
†Research Engineer, Flight Dynamics Branch, Member AIAA.
‡Research Engineer, Flight Dynamics Branch, Associate Fellow AIAA.
§Research Engineer, Associate Fellow AIAA.
¶Senior Project Manager, Projects and Engineering Branch.

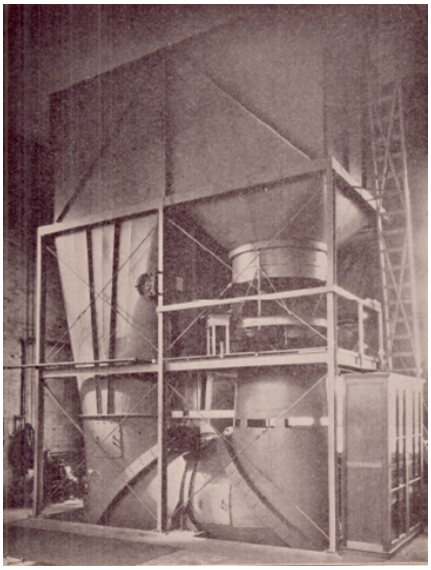

Fig. 1 5-Foot Vertical Wind Tunnel in 1931. (Credit: NASA)

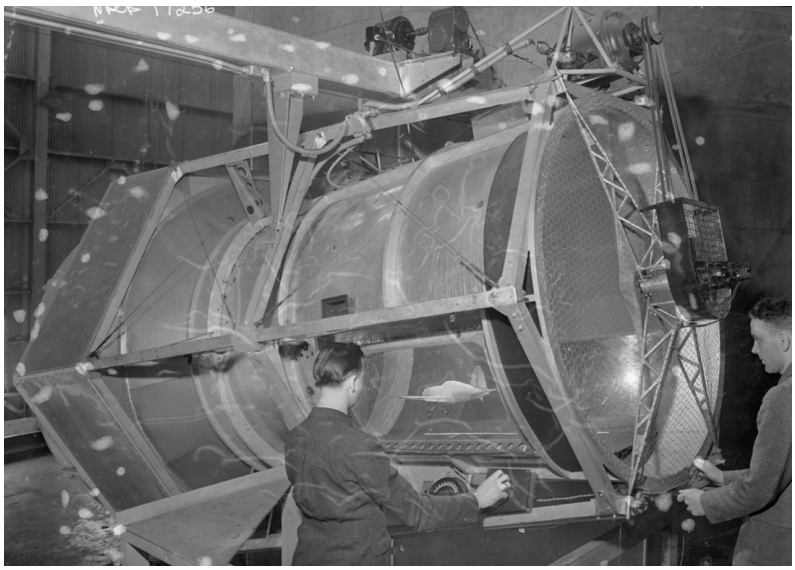

Fig. 2 5-Foot Free-Flight Tunnel, predecessor to the 12-Foot Free-Flight Tunnel, which was completed in 1937. (Credit: NASA)

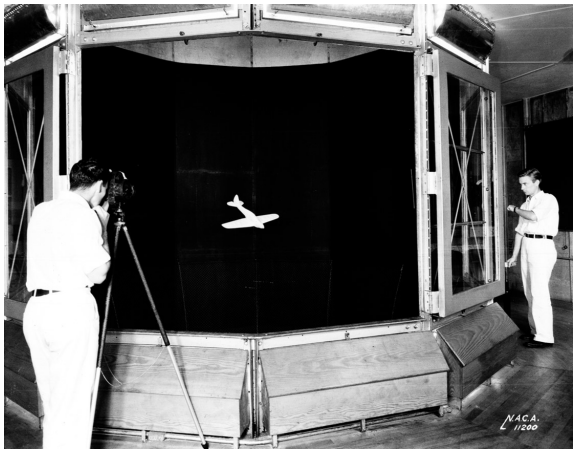

Fig. 3 Researchers testing a model in the 15-Foot Free Spinning Tunnel, which became operational in 1935. It was the predecessor of the current 20-Foot Vertical Spin Tunnel. (Credit: NASA)

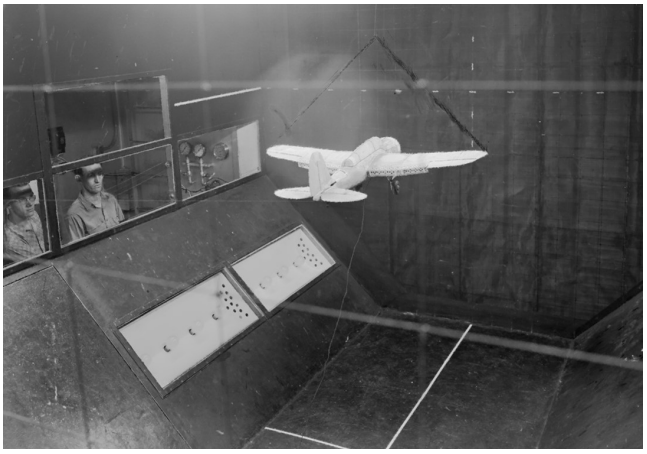

Fig. 4 12-Foot Free-Flight Tunnel in 1940. Pitch and airspeed operators are seen at left. The roll/yaw pilot is out of view in a bubble enclosure at the bottom rear of the test section. (Credit: NASA)

airspeed) divided up the task due to the fact that angular rates at model-scale are faster than those at full-scale by a multiple of the square root of the scale factor [4]. Later, models powered by electric motors were also tested. The free-flight technique was moved to the much larger Langley Full-Scale Tunnel [5] (also known as the 30-by 60-Foot Tunnel) in the late 1940s. At that time, the tilting test section in 12-Foot was fixed in a horizontal position and has since been used as a "standard" wind tunnel, albeit with a unique appearance (e.g., housed in a sixty-foot diameter sphere) and internal geometry (driven by its original design intent as a free-flight tunnel).

The current VST had two predecessor tunnels: a closed-return/open-throat vertical tunnel with a 5-foot test section equipped with a rudimentary rotary balance system for measuring forces of models undergoing "coning" to mimic motions encountered during a spin (Fig. 1), and an open-return/closed-throat vertical tunnel with a 15-foot test section (Fig. 3). The "15-Foot Free Spinning Tunnel" was conceived by Charles H. Zimmerman [2] based on knowledge that the British had developed a technique for free-flight testing of dynamically-scaled (i.e., equal Froude number and density ratio) models continually in the rising airstream of a vertical tunnel. This tunnel was housed in a tall barn-like structure

Fig. 5 Model under test in the 20-Foot Vertical Spin Tunnel in 1941, shortly after the VST became operational. (Credit: NASA)

Fig. 6 Contemporary photo of the four-building complex housing the 20-Foot Vertical Spin Tunnel and 12-Foot Low-Speed Tunnel adjacent to two support buildings that are located in the NASA Langley "East Area" on Langley Air Force Base. The large parking lot behind the complex is the site of the former Full-Scale Tunnel, which was demolished in 2011. (Credit: NASA)

to protect it from weather and minimize any effects of ambient wind on tunnel performance and test results. The building still stands today as a support building for the current VST and 12-Foot (right-most white building in Fig. 6).

The fact that the VST and 12-Foot are operating and in demand in 2024 is a testament to the flexibility and adaptability that was designed into these facilities in the 1930s. Although the designers could likely not have conceived some of the testing needs driven by 21st-century aerospace vehicles, the simple yet robust layouts and construction have allowed continual evolution of their capabilities. With continually-upgraded test rigs, data systems, and other instrumentation, the VST and 12-Foot are still supporting their original missions (airplane spin testing and stability-and-control testing, respectively), along with tests of advanced next-generation transport concepts, crewed and uncrewed Earth-entry vehicles, atmospheric entry vehicles for exploring Venus and moons of Saturn, stabilizing parachute characterization, and electric vertical takeoff and landing (eVTOL) aircraft for advanced air mobility (AAM). In large measure due to the emergence of this last category, the diversity of vehicles and other concepts continues to expand beyond the confines of traditional flight vehicles undergoing aerodynamic testing. The broad design space enabled by electric power combined with VTOL capabilities for both cargo and passenger transport has introduced a vast number of possible configuration solutions that will need to be tested in facilities like the FDRF before they can be fielded. The next section discusses some of the requirements for the new FDRF facility and capabilities that will be transferred from the current facilities to the FDRF.

III. Flight Dynamics Research Facility

The Flight Dynamics Research Facility, or FDRF, was conceived to replace both the 12-Foot Low-Speed Tunnel and the 20-Foot Vertical Spin Tunnel. The FDRF will have all of the capabilities of the two existing tunnels while also having significantly higher performance and improved flow quality compared to the two existing tunnels. FDRF was proposed to be part of the NASA Langley Revitalization Plan [6] in the early 2010s. Multiple years of design studies and vetting by various stakeholders followed before the Agencywide Flight Mechanics Capabilities Leadership Team of the NASA Engineering and Safety Center (NESC) accepted a proposal to upgrade the Agency's flight mechanics test facilities and brought the FDRF concept forward to NASA headquarters for additional vetting. In September 2021, the General Services Administration (GSA) awarded the $43.2M design-build contract to the team of B.L. Harbert International as the prime contractor, Calspan ASE (now North Wind) as the wind tunnel designer and systems integrator, and Mason &

The use of trademarks or names of manufacturers in this report is for accurate reporting and does not constitute an official endorsement, either expressed or implied, of such products or manufacturers by the National Aeronautics and Space Administration.

Hanger Group as the architecture and engineering firm. As of the writing of this paper, construction of the facility is well along, and is projected to be completed in the summer of 2025. A detailed description of the current status and a construction timeline is provided later in the paper.

A. FDRF Requirements Definition

The tunnel performance requirements, as well as those for the test equipment, site, building, and support infrastructure, were initially developed for a Preliminary Engineering Report (PER) published in late 2016 by Jacobs Engineering Group under the Langley Center Maintenance, Operations and Engineering (CMOE) contract with significant input from NASA wind-tunnel and facility construction experts. Once FDRF was funded in the NASA budget, a team of NASA (project customer), GSA (government contracting entity and project management), and Jacobs Engineering (wind tunnel design consultation, construction management, and commissioning agent) personnel was formed to solicit proposals, select the winning design-build team, and manage the project from concept definition through construction and commissioning.

One of the first tasks for the project team was to develop the official Program of Requirements (POR) that would be used to solicit proposals from potential contractors. The requirements defined in the earlier PER provided a starting point but were greatly expanded and refined to include topics such as the overall statement of work, the critical tunnel performance parameters, and the details regarding integration of government-furnished equipment (GFE) that is to be re-purposed from the existing facilities. For the wind tunnel itself, some of the important tunnel performance requirements included:

- A round or 12-sided test section with a diameter of 20 ft to 22 ft
- A controllable dynamic pressure range of 0.5 lb/ft^2 to 35 lb/ft^2
- A flat velocity profile across the core flow at the test rig elevation
- Maximum flow angularity of 0.5 deg
- Maximum longitudinal turbulence intensity of 0.5%
- Means of controlling tunnel state by open-loop (joystick) and closed-loop (dynamic pressure, airspeed, or fan RPM) methods
- Test section flow acceleration under open-loop control of at least 20 ft/s^2
- Test section flow deceleration under open-loop control of at least -10 ft/s^2
- Active cooling of the tunnel circuit

The concept of NASA providing specialized existing test equipment as GFE was one of the significant cost-saving approaches used when developing the FDRF concept. In the POR, it was specified that major systems that had been kept up-to-date and were in good working order would be re-purposed from the legacy tunnels rather than designing and building custom systems from scratch. The POR delineates several items to be integrated into the FDRF. A partial list of equipment to be removed from the 20-Foot Vertical Spin Tunnel and integrated into the FDRF includes:

- The Rotary Balance System (RBS) test rig and associated control system
- RBS forced oscillation mechanisms and associated control system
- RBS data acquisition system (DAS)
- Free-flight (optical motion-capture) DAS
- Digital video documentation cameras
- Center of Gravity/Moment of Inertia (CG/MOI), or “swing” rig
- Uninterruptable Power Supply (UPS)

A partial list of equipment to be removed from the 12-Foot Low-Speed Tunnel and integrated into the FDRF includes:

- The C-strut test rig and associated control system
- C-strut forced oscillation mechanism and associated control system
- C-strut DAS
- Electronically scanned pressure measurement system
- Smoke generation system
- Flow visualization laser light sheet system
- Digital video documentation cameras
- Uninterruptable Power Supply (UPS)

A requirement that will provide a significant improvement in tunnel efficiency, as well as the flow quality, is that the two primary test rigs (RBS and C-strut) must be fully retractable from the test section when not in use. This provides

the capability of working on model buildup on one rig while the other is inserted for testing. Alternatively, both rigs can be retracted during free-flight testing. This is an improvement over the current VST, where the RBS stored against the test section wall protrudes into the airstream and causes some flow quality degradation. Furthermore, during free-flight tests in the current VST, models are frequently damaged due to impact with the stored RBS, which will be obviated by retracting both rigs from the test section in the FDRF. Operation of the test rigs will be described in a later section of the paper.

B. Design and Layout of FDRF

The FDRF is a vertical, closed double-return, closed-throat wind tunnel. The 12-sided test section measures 20 feet across the flats and is 24.5 feet tall. The building is approximately 134 feet tall, 179 feet wide, and 95 feet deep. A simplified sketch of the tunnel circuit is shown in Fig. 7, while an artist's concept of the building exterior is shown in Fig. 8a. Some of the primary features of the tunnel circuit visible in Fig. 7 include double return legs with turning vanes in each corner; four 750 horsepower motors, each with an integrated, 14-foot diameter, eight-bladed fan equipped with carbon fiber blades (two fan-motor units per return leg); active cooling of the tunnel circuit via heat exchangers immediately downstream of the fans in each return leg; a honeycomb flow straightener; two flow-conditioning screens; a 5:1 contraction cone leading into the test section; and a high-speed diffuser immediately downstream of the test section. North Wind used proprietary wind tunnel design tools and high fidelity computational fluid dynamics (CFD) simulations to optimize the tunnel circuit, while NASA and Jacobs Engineering CFD specialists focused on analysis of design features in portions of the circuit to help ensure that unsteady flow was not of concern.

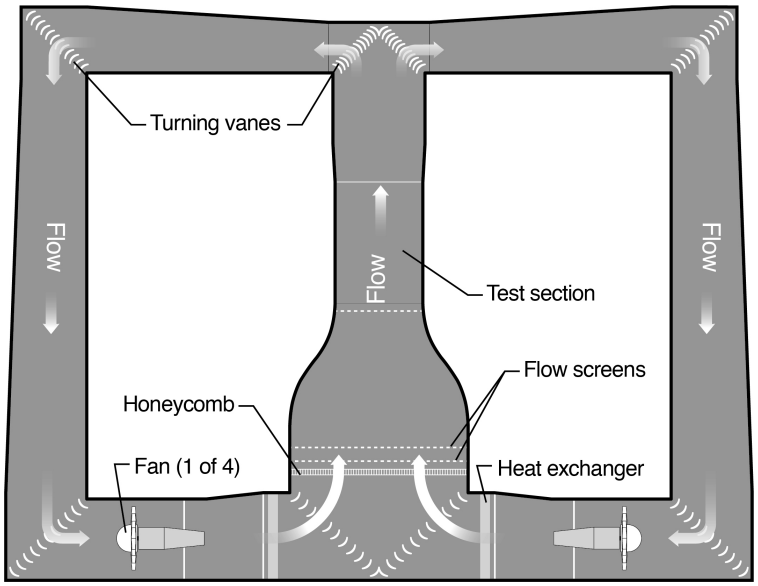

Fig. 7 Simplified tunnel circuit of the FDRF. (Courtesy of B.L. Harbert Intl. and North Wind)

Normal entry into the facility is via a lobby at the front of the building, which has both personnel entry doors as well as a large glazed rollup door for bringing in test articles and other equipment. An oversized elevator is accessed via the lobby, and is designed to double as both a passenger elevator and freight elevator. Figure 8b is an artist's concept of the entry lobby with the elevator doors visible on the left side of the image. The project has plans for a display area for test articles and images tracing the history of the current VST and 12-Foot, as well as an interactive monitor for displaying current activities and envisioned future projects. Also at ground level are "back of the house" areas for storage, machine rooms, and other support infrastructure such as telecom, electrical, mechanical, fire suppression, etc.

The control room is located at approximately halfway up the structure (note the windows shown in Fig. 8a) and is where the vast majority of the activity will take place. One of the design requirements was to maximize the amount of available space and keep the area as open and flexible as possible to preserve the successful design philosophy of the legacy facilities. Figure 9 is a plan view of the control room layout. In general, the right side of the image shows the "industrial" side of the room. This is where technicians and engineers will execute model buildup, instrument installation, and calibration, and other test-specific activities. The left side of the image includes the facility operator

(a) Exterior view from Langley Blvd

(b) Entry lobby

(c) Control room

Fig. 8 Artist's concept of FDRF. (Courtesy of B.L. Harbert Intl. and Mason & Hanger)

(closed-loop tunnel control for captive testing, test rig control, open-loop control for free-flight) and research system consoles (data acquisition, digital video feeds, data analysis), as well as space for NASA personnel and guest researchers to display data and other images while not actively operating the tunnel. At the bottom of the image are a small break area with kitchen as well as restrooms. It is also interesting to note the difference in usable space that will be available in FDRF relative to the current VST. Although the 20-foot test section diameter is the same for each facility, the difference in usable control room area is dramatic. In Fig. 9, the walls of the VST control room are represented by the red dashed circle on the FDRF plan view.

A graphic showing a view of the control room from the perspective of the researcher area looking toward the test section can be seen in Fig. 8c. The test section is designed to maximize test article observability via large windows that wrap around 120 degrees, in addition to multiple digital camera views that will be available to researchers. Other transparencies in the test section enable 16 motion capture cameras to track free-flight models under test, and an extensive LED lighting system that can be adjusted to best illuminate unique test situations. For model changes during a test, either of the test rigs can be retracted and re-injected as noted earlier, or for situations that do not require access to the entire model, a rail-mounted "deployable work platform" can be quickly extended up the center of the test section to allow a technician to make an adjustment or other minor change. Test rig and work platform operation will be discussed further in the next section.

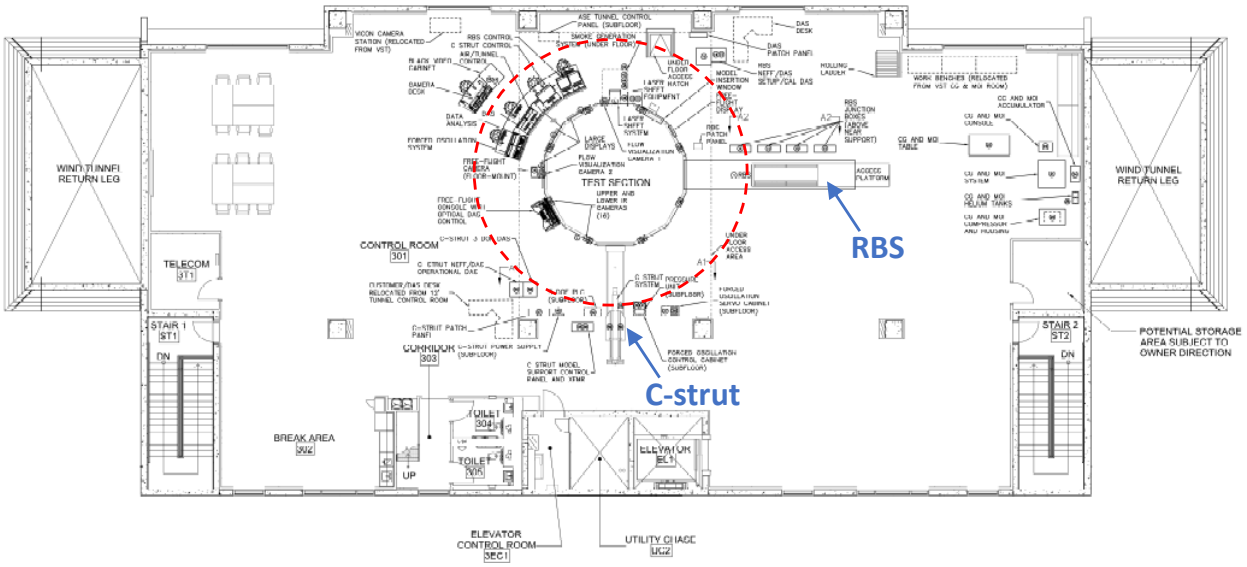

Fig. 9 FDRF control room layout. The red dashed circle represents the relative location of the outer walls of the current VST control room, which illustrates the significant size difference of the available workspace between the two facilities. (Courtesy of B.L. Harbert Intl. and North Wind)

IV. Test Rigs and Ancillary Equipment Transferred From Legacy Tunnels to FDRF

Performance and test-equipment requirements for the design and construction of FDRF were outlined in Sec. III.A. This section summarizes the standard test capabilities (i.e., test rigs and ancillary equipment) that will be repurposed from the 20-Foot Vertical Spin Tunnel and 12-Foot Low-Speed Tunnel to the FDRF. Detailed descriptions of the test techniques enabled by these rigs are provided in Sec. V.

A. Rotary Balance System (RBS)

A sketch of the RBS, as installed in the VST test section, is shown in Fig. 10. The rig is capable of performing the following types of testing:

- Static force and moment
- Sinusoidal forced oscillation
- Steady rotary coning
- Combined coning and forced oscillation
- Surface pressure measurements

As noted in Sec. III.A, the RBS in the FDRF test section is fully retractable, eliminating adverse impacts to flow quality and risk of model damage during free flight testing. Additionally, the new design allows preparations for testing using the RBS while the tunnel is in operation, significantly increasing productivity. The location of the RBS in FDRF is at the 3-o'clock position around the test section, as shown in Fig. 9. The design being constructed utilizes a motorized carriage that rides on an overhead rail system in a truss structure suspended from the control room ceiling by 28 steel attachment points embedded into the precast concrete. The RBS boom will be attached to this carriage so that an operator can inject or retract the rig through a large access hatch. A drawing of the RBS attached to the carriage and truss structure in the retracted position is shown in Fig. 11. When injected, the hatches and rig together form a smooth flow surface that is contiguous with the test section wall.

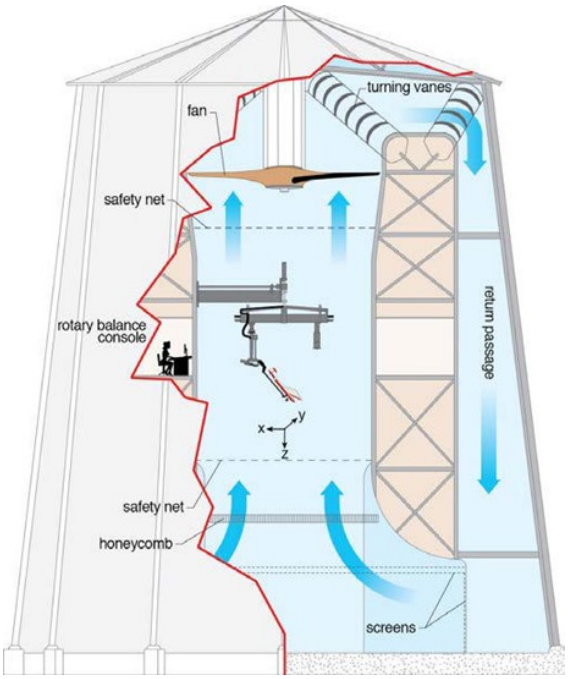

Fig. 10 Sketch of RBS installed in 20-Foot Vertical Spin Tunnel. (Credit: NASA)

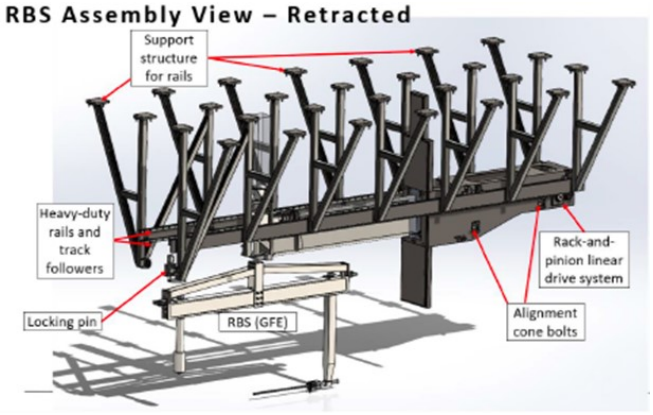

Fig. 11 Layout of RBS insertion-retraction mechanism in FDRF. (Courtesy of B.L. Harbert Intl. and North Wind)

B. C-strut

A sketch of the C-strut, as installed in the 12-Foot test section, is shown in Fig. 12. The rig is capable of performing the following types of testing:

- Static force and moment with arbitrary model attitude-pause or continually-varying model attitude
- Forced oscillation, including arbitrary motion shapes and varying frequencies
- Three degree-of-freedom (free to simultaneously roll, pitch, and/or yaw)
- Surface pressures measurements

For installation in the FDRF, the C-strut will be rotated 90 degrees from a horizontal orientation to a vertical orientation. This reorientation necessitates new hardware for yaw motion of the rig, and also cable management. Because the test section of FDRF is significantly larger than that of 12-Foot, a new horizontal mounting "boom" will extend the current mounting post and allow a test article to be positioned on the tunnel centerline. As used in 12-Foot, the C-strut stays installed in the test section unless an unconventional test type (e.g., a multirotor free-flight test [7]) needs to be utilized. In this scenario, the C-strut must be manually extracted from the test section using an overhead hoist. This operation requires two technicians and takes approximately two hours to accomplish, with an additional two hours to re-install the rig (i.e., half a shift is needed for the complete removal/installation evolution). Therefore, like the RBS, the C-strut will be mounted on an actuated rail system so that it can be injected into the test section and then fully retracted into the model build-up area (the location of the C-strut in FDRF is at the 6-o'clock position around the test section, as shown in Fig. 9). Figure 13 is a drawing of the rail-mounted carriage with extendable boom that will also provide yaw capability for the rig.

C. Flow Visualization Systems

A laser light sheet and smoke wand system will be used for flow visualization in FDRF. Figure 14 shows an example visualization of aircraft forebody vortices using the 12-Foot smoke wand/laser light sheet system. A few existing components from the system in 12-Foot will be reused, but it was decided to purchase a modern air-cooled laser to replace the existing water-cooled unit. Also, given the test section size difference between 12-Foot and FDRF, a new smoke wand will be fabricated and installed. Both the laser and the smoke will be controlled from a console in the control room to allow researchers to explore flow structures of interest while viewing video through a dedicated

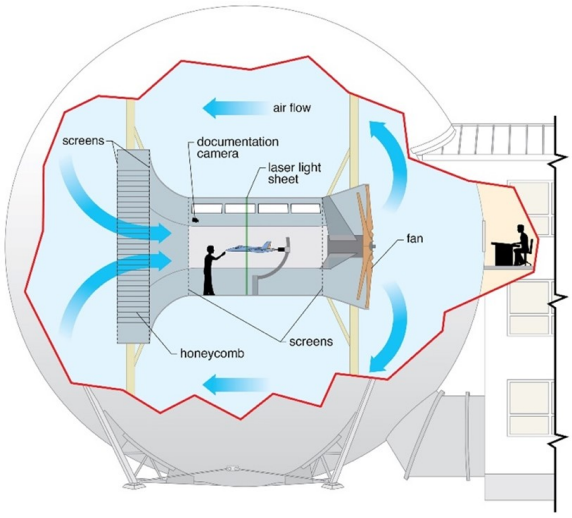

Fig. 12 Sketch of C-strut installed in 12-Foot Low-Speed Tunnel. (Credit: NASA)

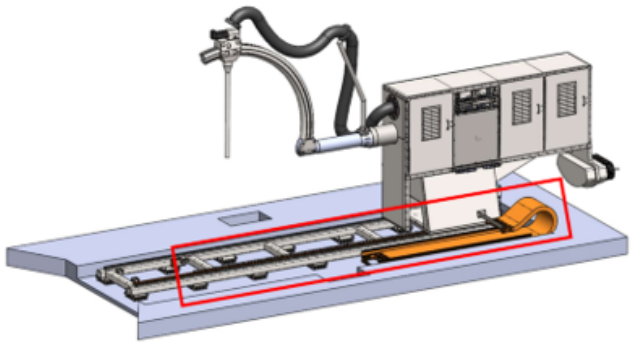

Fig. 13 Drawing of C-strut mounted on the FDRF injection/retraction mechanism. The curved tube extending to the sting and the orange device along the track (highlighted by the red box) are part of the cable management system. (Courtesy of B.L. Harbert Intl. and North Wind)

viewport. The FDRF test section will have approved laser curtains, inserts, or boxes on all transparencies, and the system will be fully interlocked to prevent operation without all safety features active. The system is designed to work with models mounted on either the C-strut or RBS (note that the RBS as currently installed in the VST does not have a flow visualization capability).

Fig. 14 Aircraft model being tested with and without flow visualization in the 12-Foot Low-Speed Tunnel. The photo on right shows forebody vortices being visualized by the smoke wand/laser light sheet system. (Credit: NASA)

D. Free Flight System

As noted in Sec. I, the VST and its immediate predecessor facility were originally designed to test dynamically-scaled, free-spinning models. That technique is still in use today for everything from traditional airplane spin testing (spin mode determination, spin-recovery characteristics, and sizing of emergency spin-recovery parachutes) to the evaluation of the dynamic stability of atmospheric entry vehicles for Earth-return, as well as for planetary science missions to Venus and Saturn's moon Titan. While engineers in the 1930s through the 1980s analyzed motion picture images of tests (and timed spin rates using a stopwatch in very early tests), beginning in the 1990s photogrammetric methods have been used to track the motion and attitude of models under test. Beginning in the mid-2000s, the VST has used off-the-shelf Vicon™ motion capture systems, which have been upgraded over that time period. While the VST uses 14

cameras (eight in the lower test section, six in the upper test section), FDRF will use a total of 16 cameras (eight low and eight upper)—the 14 cameras currently installed in the VST and two spares. Additionally, while the cameras in the VST are mounted directly on the walls of the test section (feasible due to the low maximum dynamic pressure of the facility), in FDRF they will be installed behind infrared-transparent glass that is flush with flow surfaces. A photograph of some of the cameras in the VST test section is shown in Fig. 15.

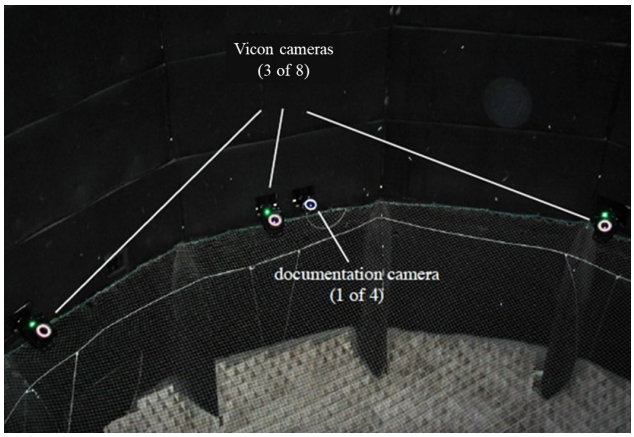

Fig. 15 Three of fourteen Vicon motion capture cameras installed in the VST. (Credit: NASA)

Fig. 16 CG/MOI measurement instrument for dynamically scaled models. (Credit: NASA)

Free flight testing also makes use of a highly accurate mass properties measurement unit, or "swing rig," to precisely determine the mass, center of gravity (CG), and moments of inertia (MOI) of a test article. Lead ballast weights are used to adjust the mass properties to match a full-scale vehicle according to dynamic scaling relationships [4] based on equal Froude number. The swing rig used at the VST will be moved to FDRF to enable free-flight testing at that facility. A photograph of the swing rig and operations console is shown in Fig. 16. The Plexiglas shroud is designed to minimize air current effects on the measurements, and also allows helium to be pumped in, displacing the air, and simulating a partial vacuum in order to estimate air damping corrections to the measured moments of inertia.

E. Surface Pressure Measurement System

Surface pressures measurements via an electronically-scanned system that are available in both the VST (on the RBS) and 12-Foot (on the C-strut) will be migrated to the FDRF. TE Connectivity DTE Initium™ hardware is used that is capable of scanning up to 512 channels via modules (mounted internally within a test article) with 16, 32, or 64 ports. Data acquisition software developed by NASA is used to interrogate pressures on forebodies, wings, control surfaces, etc. Results can be correlated with force and moment data from internally-mounted strain gauge balances or flow-visualization images to help in understanding flow physics.

V. Flight Dynamics Test Techniques

This section will describe the various flight dynamic test techniques and how the test rigs and ancillary equipment discussed in Sec. IV are employed. These test techniques include Static Force and Moment; one degree-of-freedom (1-DOF) Forced Rotational Motion with an emphasis on sinusoidal motion; Rotary Balance; Combined Motion; 1-DOF to 3-DOF Free-To-Roll, -Pitch, and/or -Yaw; and 6-DOF free-flight.

A. Static Force and Moment Testing

Static force and moment testing is primarily conducted using the C-strut rig. Static testing provides the necessary baseline for assessing the dynamic motion effects. The C-strut, pictured in Fig. 17, provides a pitch angle range from -9.5 to $+89.5$ degrees, a yaw range of ± 90 degrees, and a maximum model weight of 120 lb. The RBS, illustrated in Fig. 18, is also utilized for static testing over a large attitude range, although at lower load limits than provided by the C-strut. The RBS rig deflection ranges, rotation rates and load limits are listed in Table 1.

Fig. 17 Model mounted on the C-strut in the 12-Foot Low-Speed Tunnel. (Credit: NASA)

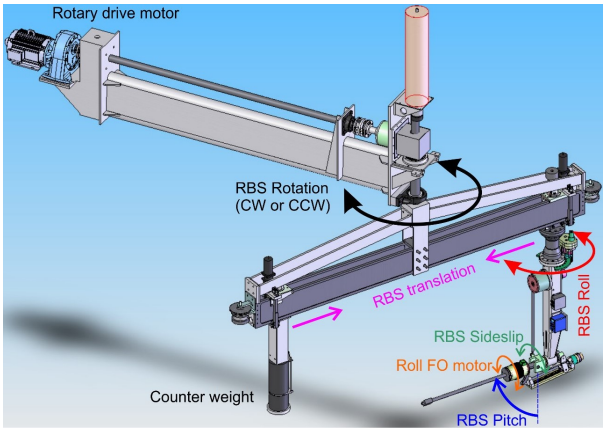

Fig. 18 Rotary-Balance System illustration. (Credit: NASA)

Table 1 RBS rates, deflection ranges, and load limits.

	Minimum	Maximum
Rotation rate, rpm	0	68 (40 with tare bag)
Pitch, deg	0	90
Roll, deg	−90	90
Sideslip, deg	−45	45
Model weight, lb*	0	15

*Maximum weight for rotary testing. Higher model weights are permitted for static testing, depending on expected loading.

B. 1-DOF Forced Rotational Motion

This test technique provides a prescribed rotational time-history motion of a test article about a fixed axis. This is generally an oscillatory sinusoidal (fixed amplitude and frequency) motion used to produce classic damping derivatives. The data processing for this technique is described in Ref. [8]; however, other rotational motions can also be utilized such as constant rate or variable frequency sweeps [9]. The rotational motions can be produced about the roll, pitch, or yaw axes. This testing can be conducted on both the RBS and C-strut. Figure 19 shows the forced-oscillation motor installed with a model on the C-strut while Fig. 20 shows the roll oscillation motor installed on the RBS. Figure 21 shows a model mounted on the C-strut in the roll, pitch, and yaw forced oscillation configurations. The C-strut motor can impart angular motion over a range of 330 deg with maximum angular rate and acceleration of 200 deg/s and 12,750 deg/s^2, respectively. The maximum oscillation frequency is 2.4 Hz.

C. Rotary Balance

Rotary-balance testing has been conducted in the VST since 1945. This test technique is used to measure rotary aerodynamic coefficients, predict spin modes, and spin recovery control authority. The current RBS has been in operation since 1992. The test model is sting mounted to the rig such that the center of rotation (typically the vehicle center of mass) is aligned with the rig axis of rotation at the desired model orientation, as illustrated in Fig. 22. The rig can rotate up to 68 rpm in a clockwise or counterclockwise direction.

Rotary balance testing, like other wind tunnel testing, requires removing the inertial forces and moments from the balance measurements to resolve the aerodynamic contributions. The difference with rotary-balance testing compared to static testing is that the wind-off tare measurements are taken with the rig and model rotating. To minimize the effect of the rotating airmass on the wind-off measurements the model is enclosed in a "tare bag," as shown in Fig. 23. A wind-off tare bag run is required for each wind-on test configuration (model configuration, attitude and rotation rate).

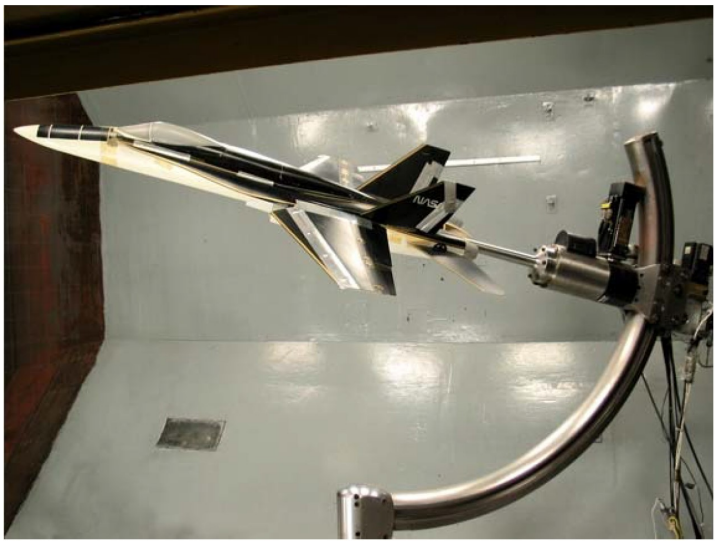

Fig. 19 Model mounted on the C-strut with forced-oscillation motor. (Credit: NASA)

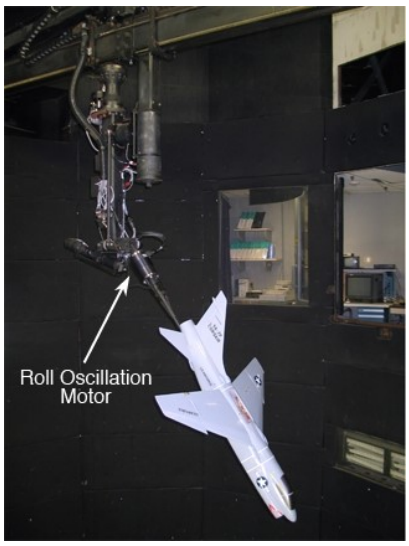

Fig. 20 Modular roll oscillation mechanism installed on the VST rotary balance. (Credit: NASA)

(a) Roll oscillation configuration **(b) Pitch oscillation configuration** **(c) Yaw oscillation configuration**

Fig. 21 Model mounted on the C-strut in each forced oscillation configuration. (Credit: NASA)

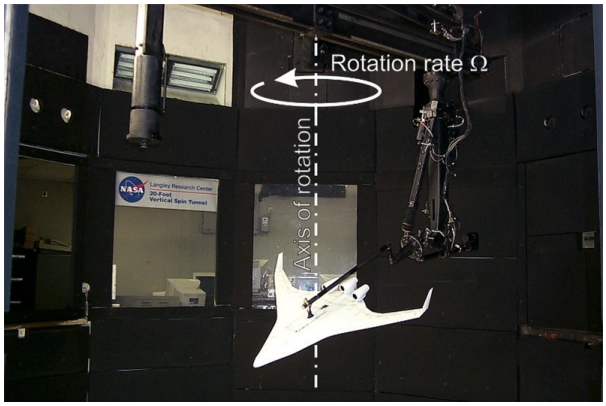

Fig. 22 Model mounted on rotary balance system. (Credit: NASA)

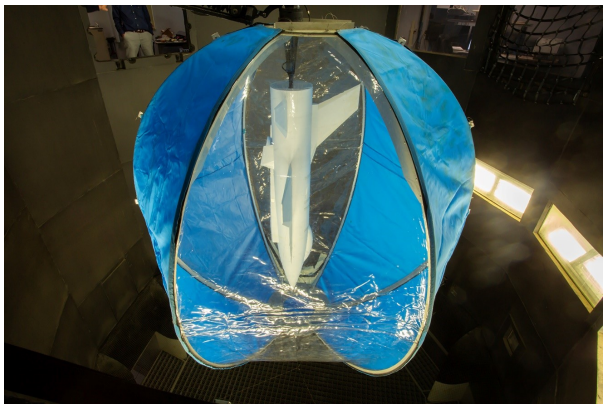

Fig. 23 Model enclosed in rotary-balance tare bag. (Credit: NASA)

D. Combined Forced Motion

Simultaneously combining a body-axis oscillation and a steady rotational coning motion can provide off-axis dynamic data to aid in simulating complex maneuvers and out-of-control modes, such as oscillatory spins. This combined motion capability is provided by adding a forced oscillation motor to the rotary balance rig, as shown in Fig. 20.

E. Three Degree-of-Freedom Free Rotation

A new three degree-of-freedom (3-DOF) test rig was designed and built in-house by the Flight Dynamics Branch at NASA LaRC in 2023. Although multiple degree-of-freedom mechanisms have been used in other facilities (e.g., see Refs. [10–15]), this is a new capability for 12-Foot that will integrate into the FDRF. The aforementioned forced oscillation and rotary balance mechanisms force the motion of a wind-tunnel model while measuring the forces and moments applied to the vehicle. In contrast, the 3-DOF rig allows for free motion in up to three rotational degrees-of-freedom where the active control effectors are used to control aircraft rotational motion. The applied moments about the rotation point are inferred from the vehicle angular velocity, angular acceleration, and moments of inertia using the rigid-body aircraft rotational dynamic equations, as opposed to being directly measured. Applied forces are not currently measured because a balance is not integrated into the 3-DOF mechanism; although, this capability could be added in future enhancements made to the 3-DOF rig. The 3-DOF rig has an encoder installed on each axis to provide aircraft orientation measurements. Rate gyroscopes can also be installed within the wind-tunnel model to provide direct angular velocity measurements.

The 3-DOF rig serves multiple purposes. The rig allows for flight control algorithms to be rapidly tested in a low-risk environment either running on a flight computer onboard the vehicle or on a desktop computer located in the control room. Based on the observations and data from free motion wind-tunnel testing, adjustments to inner-loop flight control laws can be made and verified prior to subjecting a vehicle to the risks of flight testing. Additionally, the 3-DOF rig allows for rapid extraction of aerodynamic damping derivatives by following similar analysis procedures to aircraft flight-test system identification [16]. Figure 24 shows a vehicle mounted on the 3-DOF rig in 12-Foot. The testing and subsequent analysis procedures postulated in Ref. [17] will be discussed further in Sec. VII.C.

Fig. 24 Vehicle mounted on the 3-DOF rig in the 12-Foot Low-Speed Tunnel. (Credit: NASA)

F. 6-DOF Free Flight

The free-flight dynamic test technique is used to study the 6-DOF motion of dynamically-scaled models, as shown in Fig. 25. The free-flight technique has been used in all prior vertical tunnels at NASA LaRC for both aircraft and spacecraft. The technique is used to characterize flight modes such as aircraft spins and capsule dynamics during entry, descent, and landing (EDL). Data acquisition consists of tunnel freestream conditions and trajectory capture via photogrammetry. The acquired free-flight data can be used for extracting aerodynamic models using system identification techniques [16]. The flight-derived aerodynamic models are then used along with the aerodynamic models from the captive test techniques, described above, to provide in-depth knowledge of the flight dynamics.

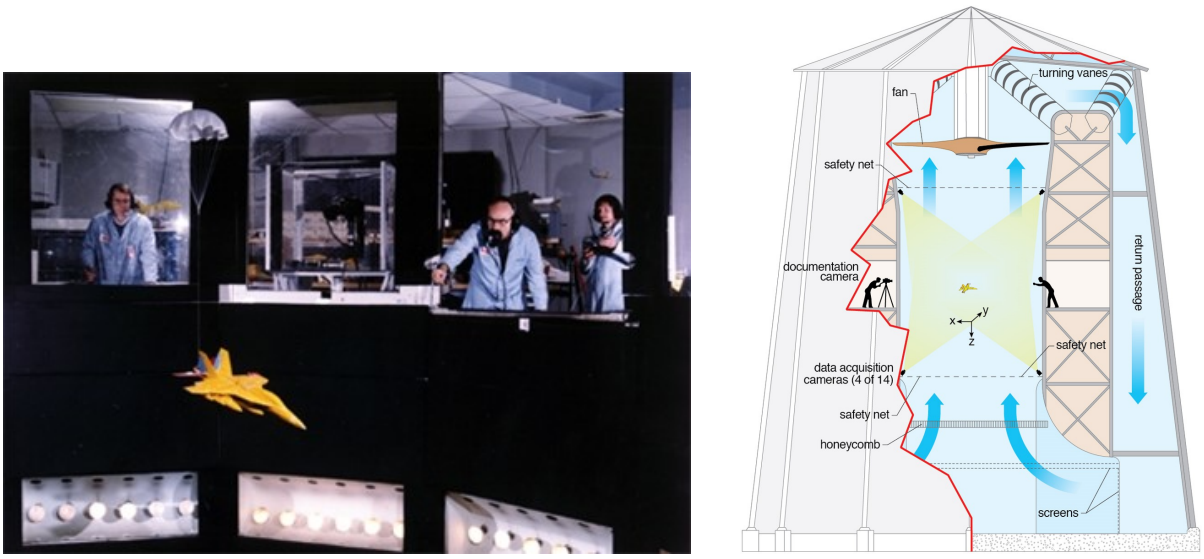

Fig. 25 Free-spin test of dynamically-scaled fighter model in the VST. (Credit: NASA)

VI. Check Standard Testing

A series of check standard tests were conducted on the legacy dynamic test rigs to provide comparison data for the FDRF rig installations. Two check standard models were developed for these tests. One is a generic fighter configuration with a low aspect ratio wing and sharp leading-edge airfoils call the Standard Dynamics Model (SDM). The other is a high aspect ratio transonic generic transport configuration called the Common Research Model (CRM). Both model configurations have been tested extensively in other facilities providing comparative data.

A. Common Research Model

The Common Research Model (CRM) is a generic twin-engine transport configuration with a transonic supercritical wing. The configuration was developed to provide experimental data for computational fluid dynamics (CFD) validation workshops [18–25]. The focus of most of the early tests and analysis was on high Reynolds number drag prediction. This original version of the CRM did not include a vertical tail and did not include any sideslip testing because the focus was on performance prediction and not on stability and control. ONERA, the French Aerospace Lab, built and tested a version of the CRM that included a vertical tail design [23]. The CRM check-standard model developed for this low-speed testing is the same loft as the original CRM configuration with the ONERA designed vertical tail and without the engine nacelles and pylons. The model was fabricated using a polycarbonate rapid prototyping technique. This fabrication technique provided an accurate replication of the geometric details while meeting the stringent and challenging mass properties targets required for dynamic testing. A three-view drawing and photo of the CRM model are shown in Figs. 26a and 26c. The model reference values and weight are listed in Table 2.

Table 2 Check standard CRM and SDM reference geometry and mass properties

Property	CRM	SDM
Wing area (S), ft^2	2.379	4.797
Wingspan (b), ft	4.627	3.795
Mean aerodynamic chord ($\bar{c}$), ft	0.552	1.431
Weight, lb	15.85	13.35

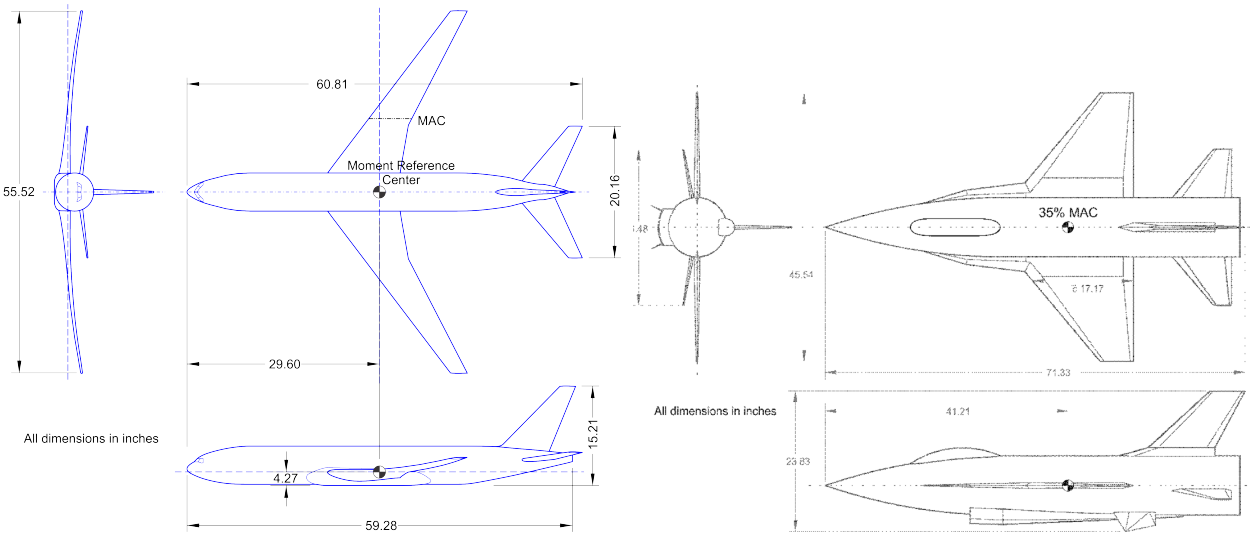

(a) CRM geometry **(b) SDM geometry**

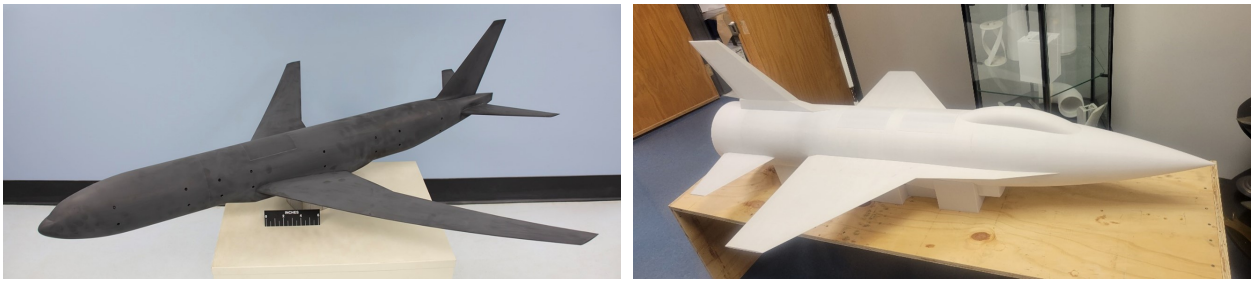

(c) CRM photograph **(d) SDM photograph**

Fig. 26 FDRF CRM and SDM check standard models. (Credit: NASA)

B. Standard Dynamics Model

The Standard Dynamics Model (SDM) is a generic F-16 like fighter configuration that has been tested in various tunnels both statically and dynamically. The model configuration was developed by the Unsteady Aerodynamics Laboratory of the National Research Council of Canada in October 1978 [26]. It is a simple geometry of which several models of various sizes have been produced and tested throughout the world [26–42]. A three-view drawing and photo of the model are shown in Figs. 26b and 26d. The model was fabricated using the same polycarbonate rapid prototyping technique used for the CRM. The model reference values and weight are listed in Table 2.

VII. Advanced Test Techniques

This section describes advanced test techniques that have been applied in the 12-Foot Low-Speed Tunnel and 20-Foot Vertical Spin Tunnel. Each of these test capabilities will be employed by future FDRF test campaigns.

A. Design of Experiments

Traditional aircraft aerodynamic characterization methods generally involve using one-factor-at-a-time (OFAT) experiments, where testing is commonly conducted by sweeping one variable with the other variables held at a constant setting. This approach has been used successfully for many years in aerospace testing and yields suitable results for conventional aerospace vehicles. However, traditional static OFAT testing is not practical for characterizing aircraft with many interacting control effectors and complex nonlinear aerodynamics, such as distributed propulsion aircraft configurations intended for AAM applications. Experiments planned using design of experiments (DOE) theory [43, 44], however, can scale to a large number of factors allowing wind-tunnel tests to be completed efficiently

while supporting identification of interaction effects. DOE in this context is intended to refer to application of statistically-designed experiments and the use of response surface methods (RSM). DOE-based testing fundamentally provides a statistically-rigorous experiment design approach supplying rich information content in a relatively compact data set. The aerodynamic model development process also benefits from properties of *orthogonality*, *randomization*, *replication*, *blocking*, and *sequential testing* [43]. Nearly *orthogonal* experimental factors aid the model structure identification and parameter estimation process by ensuring low candidate regressor correlation. *Randomization* of test points reduces the effects of systematic measurement errors and extraneous factors—errors are reflected in the parameter variance rather than corrupting the parameter estimates. *Replication* of data points provides insight into the measurement facility noise characteristics. *Blocking* minimizes the effects of unmodeled nuisance factors. *Sequential testing* allows efficient data collection to obtain the desired modeling fidelity.

As a demonstration of the efficiency gains realized using DOE techniques (adapted from an example described in Ref. [45]), consider a complex aircraft with 20 independent test factors. OFAT testing covering all possible combinations of each test factor at three different levels (a low, medium, and high value) requires approximately 3.5 billion test points. Alternatively, DOE-based testing requires only on the order of hundreds of test points. For example, a minimum-run resolution V, face-centered central composite design (CCD) with one center point, which also tests three levels of each factor and allows characterization of interactions among all pairs of test factors as well as quadratic response variation with each test factor, requires only 253 test points. A two-dimensional and three-dimensional slice of the OFAT and face-centered CCD factor space are shown in Figs. 27a-27b. This example comparing the number of test points for a three-level OFAT and CCD test matrix is expanded to between 5 and 30 test factors in Fig. 27c. Application of the CCD response surface design has substantially reduced the number of required test points, while still allowing characterization of nonlinear, interactional features.

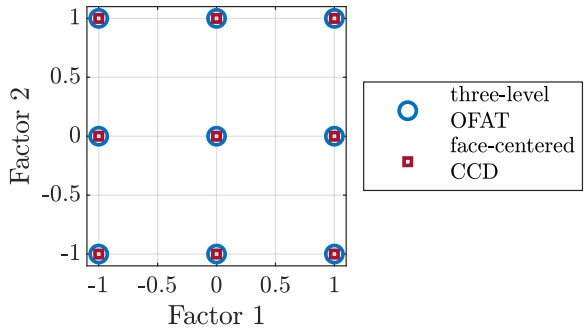

(a) Two-dimensional design space slice

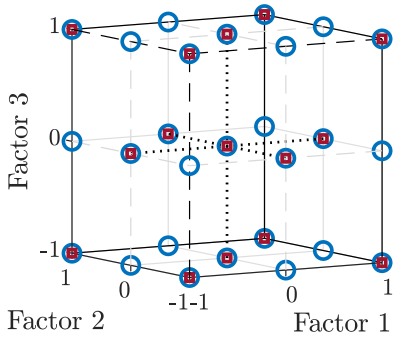

(b) Three-dimensional design space slice

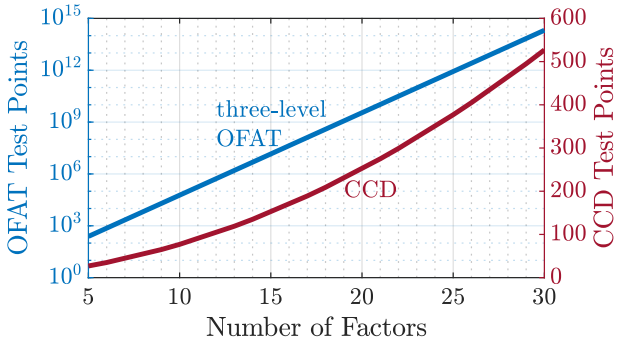

Test Factors	OFAT Points	CCD Points
5	243	27
10	~59,000	77
15	~14.3 million	153
20	~3.49 billion	253
25	~847 billion	377
30	~206 trillion	527

(c) Number of test points

Fig. 27 Comparison of three-level OFAT and minimum run resolution V, face-centered CCD experiments.

According to Ref. [46], first application of modern DOE at NASA LaRC wind tunnels occurred in 1997, which demonstrated efficiency and data quality improvements. The first test to apply DOE techniques in 12-Foot occurred in 2002 for an off-the-self, radio controlled, fixed-wing aircraft [47]. For this test, both control effectors and aircraft orientation were independently varied. The control effectors were automatically commanded by a laptop computer

independent of the wind-tunnel computer system. The angle of attack and sideslip angle had to be manually set using a joystick in the control room because, at the time, the wind tunnel computer systems were designed to only conduct OFAT experiments in an automated manner. In 2013, software upgrades accompanying the GL-10 test campaign enabled automatically commanding both orientation angles and control effector settings specified by a DOE test matrix provided to the wind tunnel computer system [48, 49]. These tunnel computer system upgrades made conducting DOE testing in 12-Foot substantially easier and led to expansion application of DOE test techniques in that facility [50–55]. The Research Aircraft for eVTOL Enabling Technologies (RAVEN) Subscale Wind-Tunnel and Flight Test (SWFT) model was the first vehicle tested in 12-Foot that employed primarily DOE techniques throughout its static test campaign, including data collection for aero-propulsive model development and other necessary parts of the test, such as gravitational tare characterization and transition trim envelope determination [54], as well as isolated proprotor testing [53]. Although DOE test techniques have mainly been applied to static wind tunnel testing in 12-Foot, recent software updates have also enabled DOE-based forced oscillation testing.

The software upgrades that enabled conducting streamlined testing using DOE test techniques will be included in the FDRF tunnel control system. Additionally, the FDRF will be able to quickly and automatically command tunnel dynamic pressure changes, which will allow dynamic pressure to be used as an easy-to-change test factor; whereas, in 12-Foot, tunnel dynamic pressure had to be treated as a hard-to-change test factor [53]. The aforementioned check standard testing included both static and forced oscillation DOE testing as a supplement to the primary check standard data acquired using OFAT techniques. These same methods will be applied in initial check standard testing conducted in FDRF.

B. Programmed Test Inputs

Another recent capability enhancement in 12-Foot is the ability to apply programmed test input (PTI) excitations during wind tunnel experiments. PTIs in the form of orthogonal phase-optimized multisine inputs [16, 56–58] are commonly applied in flight-test experiments [59], and were implemented into 12-Foot tests to increase test efficiency. A multisine input is defined as a sum of multiple sinusoidal functions with different amplitudes, frequencies, and phase angles, where the frequencies are chosen to encompass the frequency range corresponding to the system dynamics of interest. To make all inputs orthogonal in both the time domain and frequency domain, each multisine signal is assigned sinusoids with a unique subset of discrete harmonic frequency components. Because multiple inputs are simultaneously excited, the use of multisine inputs allows for execution of highly efficient and informative testing. Time histories and input spectra for an example three-input multisine design are shown in Fig. 28.

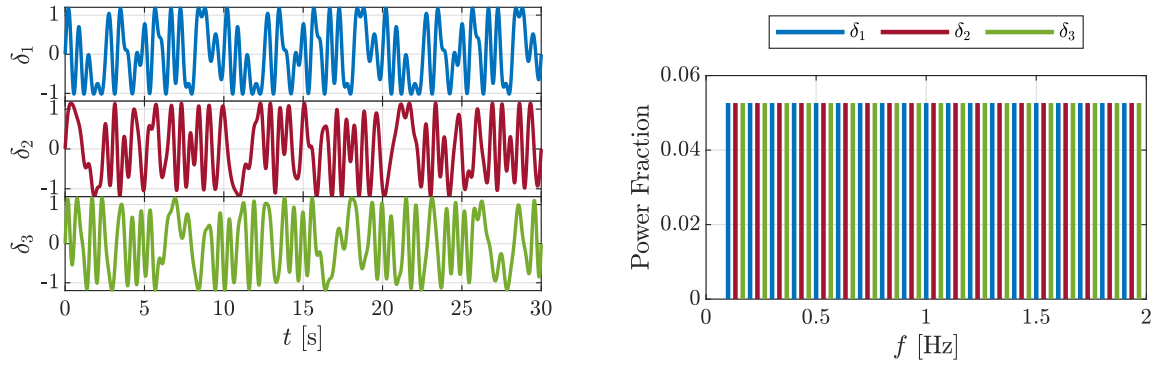

(a) Normalized time-domain signals **(b) Input spectra**

Fig. 28 Example three-input orthogonal phase-optimized multisine design.

Similar to DOE test techniques, wind-tunnel computer system upgrades were required to enable PTIs to be used in wind-tunnel testing. The first test to apply PTI excitations on control surfaces during exploratory 12-Foot testing for a fixed-wing aircraft is described in Ref. [60]. This initial study was expanded and refined in Ref. [61] for the LA-8 eVTOL aircraft, which has 20 independent control effectors and significant aero-propulsive coupling. An efficient wind-tunnel experiment was conducted using a combination of a DOE test matrix applied to slow moving test variables and PTI excitations applied to fast moving control effectors. Testing was conducted by applying DOE and PTI experiment design methods simultaneously to collect informative wind-tunnel data subsequently used for model identification. A new,

multistep model identification strategy employed frequency-domain and weighted least-squares regression methods for model structure determination and parameter estimation to combine the data information content acquired from the simultaneously applied DOE and PTI test techniques. The amount of required test time using combined DOE and PTI techniques was reduced by a factor of five compared to static DOE wind-tunnel testing for the LA-8 aircraft, which was already vastly more efficient compared to using OFAT testing for this complex vehicle, while yielding models with similar prediction capability. In addition to reduced test time, this testing and modeling approach allows for characterization of more complex nonlinear phenomena that cannot be efficiently captured in alternative modeling approaches.

C. 3-DOF Dynamic Derivative Identification

As mentioned in Sec. V.E, free motion testing on the 3-DOF rig enables efficient determination of aerodynamic damping derivatives, as well as evaluation of flight control algorithms. RAVEN-SWFT is shown mounted on the 3-DOF rig in 12-Foot in Fig. 24 and was the first vehicle to use the 3-DOF rig as a part of its wind-tunnel testing efforts [17]. The RAVEN-SWFT 3-DOF free motion test was used to verify the functionality of custom flight control software that will be used in future flight testing, assess the performance of the inner-loop flight control laws, and collect data to determine aerodynamic damping derivatives. Custom control logic was created in Simulink® and deployed to a Pixhawk flight computer onboard the vehicle. The 3-DOF test was conducted using a handheld radio control transmitter and a ground control station computer to remotely communicate with the vehicle.

Reference [17] presented a new 3-DOF free motion wind-tunnel testing and aero-propulsive model identification strategy for the RAVEN-SWFT, which can be extended to many aeronautical vehicles. To execute the RAVEN-SWFT 3-DOF test, a model-based control system was developed to stabilize the aircraft, track attitude commands, and transition the vehicle based on freestream dynamic pressure. While the flight controller was active, orthogonal phase-optimized multisine PTI excitations were injected into the attitude and control effector commands, as shown in Fig. 29, to perturb the aircraft around the reference flight condition and collect informative data for model identification. The multiple-input experiment design simultaneously excites the aircraft dynamics in all axes, resulting in very efficient testing. Multisine maneuvers were collected at multiple dynamic pressure settings across the RAVEN-SWFT transition envelope. The wind-tunnel data collection time used for modeling a single reference flight condition took under 10 minutes (with a minimum required amount of test time with PTI excitations enabled of under one minute), while still providing data enabling accurate characterization of the dominant aero-propulsive damping effects exerted on the vehicle.

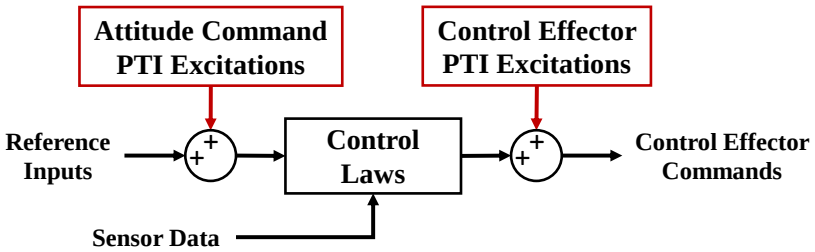

Fig. 29 PTI injections relative to the control laws used for 3-DOF free motion wind tunnel testing.

Dynamic aero-propulsive models were identified from the wind-tunnel data acquired at each tested dynamic pressure setting to produce a transition model for the RAVEN-SWFT vehicle. The form of the model is a set of polynomial response surface equations that describe the variation of the aero-propulsive moments as a function of state and control variables. The model structure for each response variable at each test condition was determined using stepwise regression [16, 62] and the model parameters were estimated using complex least-squares regression [16, 63]. The model parameters of primary interest were those involving angular velocity to quantify the quasi-steady aerodynamic damping effects (e.g., L_p, M_q, N_r, etc.) to supplement models created from previous static RAVEN-SWFT wind-tunnel testing [54]. Aero-propulsive damping derivatives were accurately determined throughout the test envelope using the approach outlined here and described in further detail in Ref. [17].

D. Entry Vehicle Dynamic Testing

The tests conducted in the VST for NASA's Orion program by its Aerosciences group will be used to exemplify the rigs capabilities and test techniques described in Secs. IV-V, for a comprehensive dynamic stability characterization.

During atmospheric EDL, blunt-body vehicles, especially ones with a backshell and large shoulder radius, are known for their dynamically instabilities. These dynamic instabilities, if left unchecked, cause large amplitude dynamics which cause the vehicle to tumble, resulting in potential loss of the vehicle, mission, and/or life. The susceptibility to tumbling typically increases as the capsule decelerates through the transonic and subsonic flight regimes. Even if the vehicle uses active controls for stability, it will eventually deploy drogue parachutes (typically, $M < 1.5$) to decelerate and maintain stability. For various reasons, the dynamics during flight under drogues can fail to meet mission requirements. Therefore, it is of paramount importance to understand the capsule's dynamic stability characteristics both for free-flight and flight under parachutes.

In addition to providing comprehensive dynamic stability characterization, the VST techniques and tunnel costs are relatively inexpensive and can be deployed rapidly. Leveraging these advantages, the Orion Aerosciences group returned to the VST multiple times to determine the effects of changes in vehicle outer mold line (OML), mass properties, and concept of operations. Furthermore, models of the Orion Crew Module (CM) and Launch Abort Vehicle (LAV) were tested in the Transonic Dynamics Tunnel (TDT) to obtain dynamic aerodynamic data at a higher Reynolds number for $M < 1.1$. The VST test results helped to optimize the use of TDT test time, which is expensive and limited due to the high demand.

The Orion program used static force and moment, 1-DOF forced oscillation, and 2-DOF captive combined motion (Fig. 30), as well as 6-DOF free-flight test techniques (Fig. 31), for the following vehicles shown in Fig. 32:

1) Crew Module (CM) (with and without simulated drogue parachutes) (Figs. 33-35)
2) Launch Abort Vehicle (LAV)
3) Launch Abort Tower (LAT) (Fig. 36)
4) Forward Bay Cover (FBC) (Fig. 37)

The VST captive test techniques allow direct measurement of the forces and moments during dynamic motion of the model over a large attitude range. As seen in Fig. 32, LAV dynamic stability must be characterized for a total angle of attack range of 0 to 180 deg. After the LAT is jettisoned, the CM experiences a brief period of free flight followed by the deployment of the drogues. During these flight phases, the CM will experience a large range of alpha and beta (> 60 deg) along with large amplitude (> 30 deg) oscillatory dynamics about the pitch and yaw axis coupled to a quasi-steady-state roll rate. The reduced frequency of the oscillatory motion will change significantly as the CM goes from free flight to main parachute inflation. The RBS system, described in Sec. IV.A can provide this multi-axis motion at dynamic similitude. Furthermore, the forces and moments of the drogues were measured, using a small six-component strain gauge balance (Fig. 38) independent of the CM. This balance was designed specifically for the parachutes used in the VST. The data from the captive techniques are used to populate the aerodynamic database with aerodynamic coefficients valid over a large parameter space. An aerodynamic database with an extensive parameter space is needed for the Monte Carlo simulation studies used by Orion to assess design metrics.

The 6-DOF free-flight test data are used to validate the dynamic aerodynamic model derived from 1-DOF methods. The free-flight data can be used to assess phenomena such as interference effects and aerodynamics induced by multi-axis motion. With its large 20-foot diameter by 25-foot high test section, the VST free-flight tests are capable of modeling lifting trajectories and tumble (Figs. 37 and 39). The free-flight methods allow for the best representation of the full 6-DOF motion at the cost of having to derive the damping from the vehicle states using parameter identification methods, such as those described in Ref. [16].

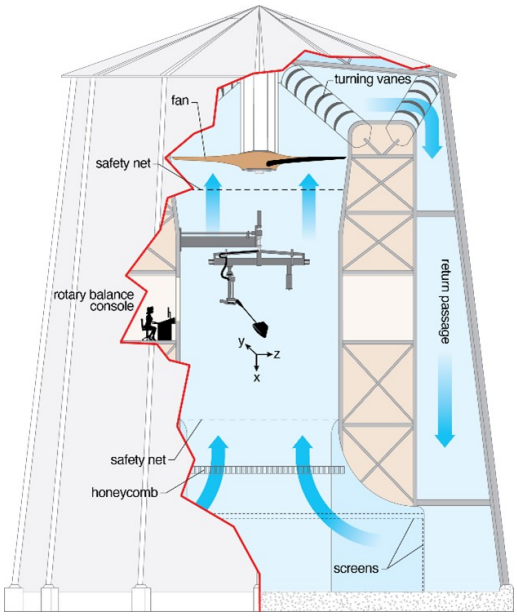

Fig. 30 Sketch illustrating the CM mounted to the RBS for static force and moment, forced oscillation, and combined motion testing in the VST. (Credit: NASA)

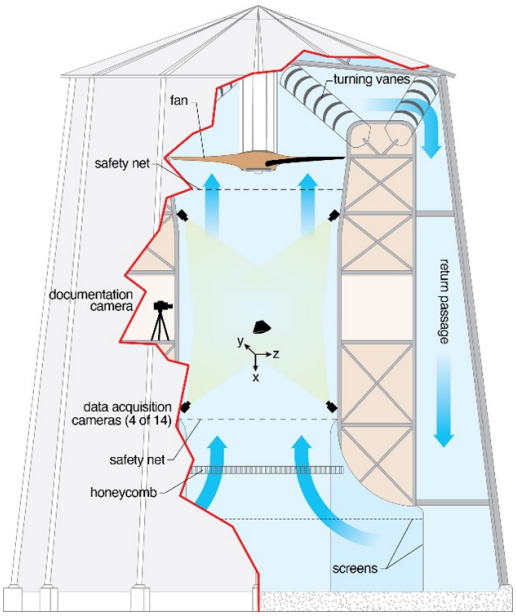

Fig. 31 Sketch illustrating the CM 6-DOF free-flight technique in the VST. (Credit: NASA)

Fig. 32 Illustration of the Orion Crew Module, Launch Abort Tower, Launch Abort Vehicle, and Forward Bay Cover. (Credit: NASA)

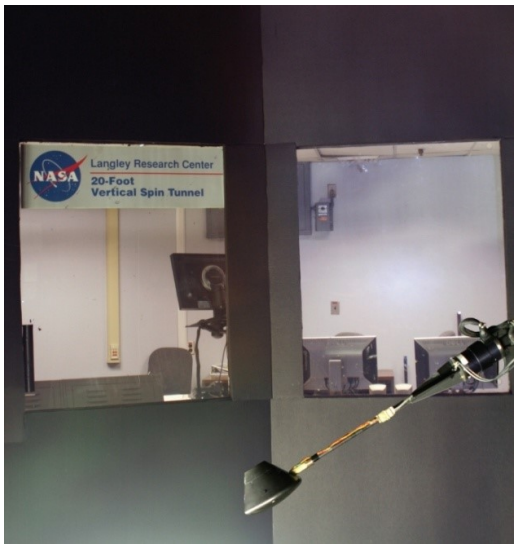

Fig. 33 Test setup for the CM static and forced oscillation test technique in the VST. (Credit: NASA)

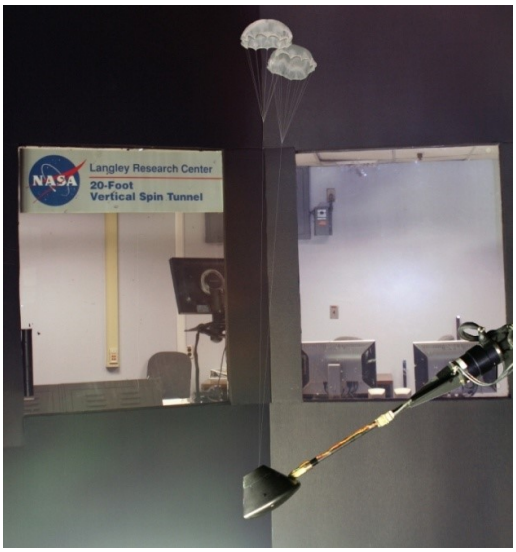

Fig. 34 Test setup for the CM with drogues deployed static and forced oscillation test techniques using a two-balance system. (Credit: NASA)

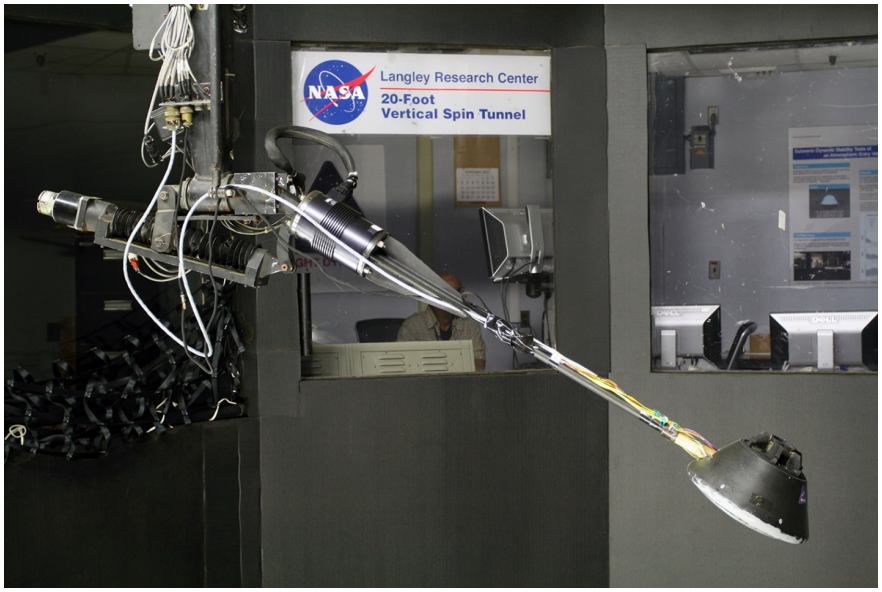

Fig. 35 6.25% Orion CM undergoing combined motion in the VST. (Credit: NASA)

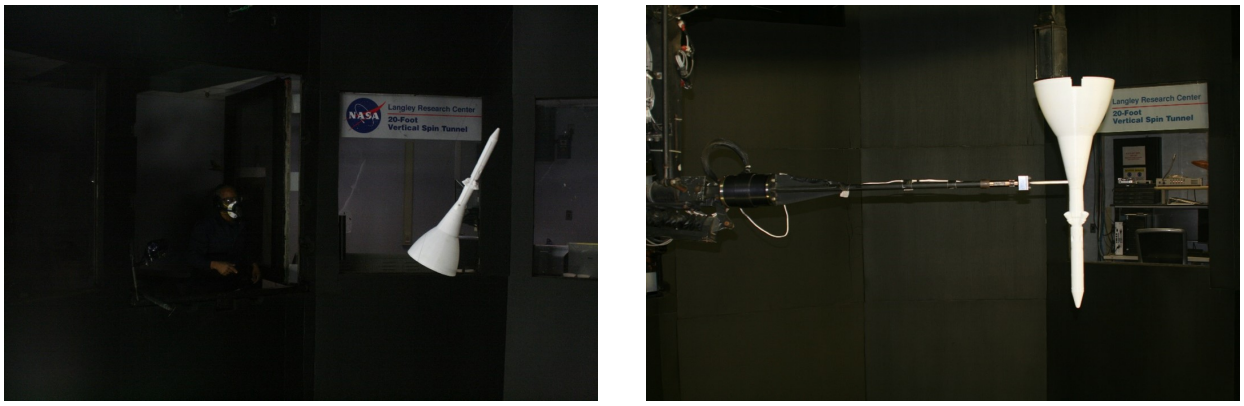

Fig. 36 LAT captive testing. (Credit: NASA)

Fig. 37 FBC conducting free-flight test after jettison from the CM. (Credit: NASA)

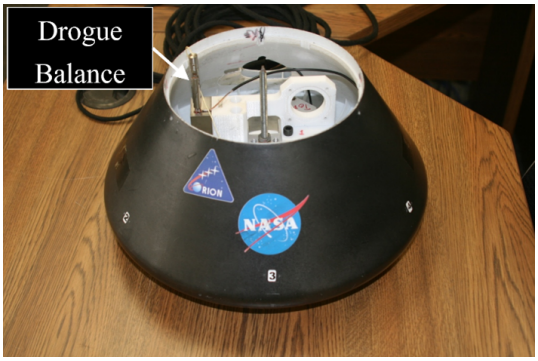

Fig. 38 CM captive model showing six-component strain gauge balance used to measure the drogue forces and moments independent of the CM and drogue system. (Credit: NASA)

Fig. 39 CM flight under drogues. (Credit: NASA)

VIII. FDRF Construction and Anticipated Operational Timeline

A. Project Procurement

NASA Langley's Revitalization program has a successful history of delivering new facilities through an interagency support agreement with the GSA. Building upon these successes, NASA teamed with GSA to execute a design-build contract for the procurement of FDRF.

In a design-build project, the prime contractor is responsible for both the design and the ultimate construction of the facility. This differs from the more traditional design-bid-build delivery method in which a design contract first delivers a complete facility design package. Contractor teams then submit construction proposals based on that design. By obtaining the design and construction through a single contract, design-build engages the construction team early in the design process. Early engagement tends to create a better understanding of project requirements and interests, allows for greater collaboration and innovation, and produces higher-levels of buy-in by the delivery team members. This delivery method also tends to shorten the overall project delivery time, enabling concurrent design and construction activity, often with less cost and schedule growth over the project life-cycle.

B. Construction Phasing

One of the more important project interests involved minimizing disruption to ongoing research mission activities. Most of the research equipment destined for FDRF is actively supporting research in the two legacy test facilities at the time of writing this paper, and some of the equipment, including the C-strut and RBS test rigs, require extensive modifications for installation in FDRF. To minimize disruptions to research, the FDRF contract stipulated a two-phase construction process. Construction Phase 1 will deliver a fully-functional vertical wind tunnel, with an empty test section, along with the commissioned building systems (environmental control, fire detection and suppression, and security). The subsequent Phase 2 includes the removal, modification, installation, and commissioning of the research equipment relocating from the legacy facilities.

C. Progress to Date

GSA awarded the design-build construction contract in September 2021 to the team of B.L. Harbert International, Mason & Hanger Group, and Calspan ASE (now North Wind). The team's proposal included a 10% concept design for the facility and the first significant windfall from the design-build process. While exploring ways to reduce overall facility cost, the design team arrived at a structural concept consisting predominantly of prestressed, precast concrete. This design choice reduced overall construction cost and schedule and is projected to reduce operating and maintenance costs over the facility's life span.

Over the next two months, the design matured to a 30% concept design, presented for formal review by the government team. Working in support of the designers, the general contractor and major subcontractors identified environmental factors that posed significant schedule and budget risks to the project. Towards the end of 2021, the world was still emerging from the COVID-19 pandemic and the pace of reemergence created significant challenges throughout the global supply chain. Prices for most construction materials were increasing, some plateauing 40% higher the following year. A concurrent global semiconductor shortage caused major equipment lead times to increase two to threefold, exceeding a year in many cases.

Fortunately, design-build delivery provides for concurrent design and construction activities. With agreement by the government team, B.L. Harbert's team quickly identified items prone to cost and schedule volatility and prioritized aspects of the design around them. Those "fast tracked" design packages allowed for the early ordering of materials and equipment, securing delivery dates that met overall schedule goals and locking in pricing before it could rise further. In total, four packages were fast-tracked through the design process, while the rest of the facility design continued alongside. Those packages included:

- Package A (March/April 2022): Site development, foundations, and wind tunnel drive system (fans, motors, and variable frequency drives).
- Package B (May/June 2022): Precast building superstructure and major components of the flow path, including contraction, heat exchangers, turning vanes, and flow straightening honeycomb and conditioning screens.
- Package C (July/August 2022): Significantly longer lead time equipment, including medium voltage transformer substations, switchgear, chiller, and elevator.
- Package D (September 2022): All remaining electrical and mechanical equipment that wasn't readily available off-the-shelf.

With the fast-tracked design packages completed and long-lead time items on order or in fabrication, construction was cleared to commence in August 2022, while the design team continued apace to complete the remaining design elements. Throughout the fall and winter of 2022, the construction team completed rough sitework, drove the deep pile foundations, and cast the shallow foundations and slabs for the building. Off-site, at a dozen different locations across the U.S. and Europe, fabrication shops began building and testing the fast-tracked items. Figure 40 shows a series of photographs of the FDRF construction progress over time.

(a) Mobilization, June 2022

(b) Foundation construction, Nov. 2022

(c) Slab placement, Feb. 2023

(d) Precast erection, Apr. 2023

(e) Fan installation, July 2023

(f) Contraction cone, Aug. 2023

(g) Before test section install, Oct. 2023

(h) FDRF exterior, Jan. 2024

(i) FDRF exterior, Apr. 2024

Fig. 40 FDRF site construction progress. (Credit: NASA)

D. Current Status

As of October 2024, the 16,000 square foot FDRF building structure and envelope is complete. Figure 41 shows photos of the FDRF interior construction progress. Figure 42 shows a photo of the east fan inlets. Outside, crews are completing final grading of the site and preparing for landscaping. All equipment has been delivered, installed, and crews are meticulously working through startup procedures. Inside, crews are installing finishes, including flooring, fixtures, and final paint. Offsite, North Wind is completing the fabrication of hardware components and developing software needed to adapt the existing research equipment to the new facility.

(a) Control room **(b) Rotary balance support framing and test section**

Fig. 41 FDRF interior construction progress, October 2024. (Credit: NASA)

Fig. 42 FDRF east fan inlets. (Credit: NASA)

E. Remaining work

Phase 1 construction will conclude in December 2024, with commissioning of the empty wind tunnel in January 2025. While tunnel acceptance testing is underway, a reduced construction crew will deliver and install all of the newly fabricated assemblies to support research at FDRF. Once the new tunnel has met the requisite acceptance criteria, these same crews will begin Phase 2 by removing, modifying, and reinstalling the government furnished research equipment—test rigs and ancillary equipment—from the legacy tunnels. This work is expected to take place in the winter and spring, concluding by the summer of 2025.

F. Projected Operational Readiness

Upon completing installation of the research equipment, the design-builder's lead for wind tunnel design and equipment integration will complete a series of verification, validation, and acceptance tests, as well as training on the facility control systems. Concurrently, NASA engineers from Facilities Management and Safety and Mission Assurance disciplines will review and approve the proposed operating procedures for the facility. The design-build contract formally concludes upon successful completion of acceptance testing and operating procedures, tentatively slated for early summer of 2025.

IX. Concluding Remarks

When it becomes operational in the summer of 2025, the NASA Flight Dynamics Research Facility (FDRF) at Langley Research Center will be the first major wind tunnel built by the Agency in over 40 years, and will replace two existing tunnels that have been in continual operation since before the entry of the United States into World War II. This large, subsonic tunnel with a vertical test section was conceived for conducting all manner of flight dynamics research, from static and dynamic stability and controllability, to atmospheric entry vehicle dynamic stability, and aircraft spin and spin-recovery characterization. The designers of the 20-Foot Vertical Spin Tunnel and 12-Foot Low-Speed Tunnel could not have envisioned those facilities evolving to test supersonic aircraft, spacecraft, and advanced air mobility vehicles. Early advocates for FDRF took a cue from the longevity of the legacy tunnels as well as the demand for those facilities and made maximum flexibility and adaptability watchwords during FDRF design to help ensure that it remains an enabling facility for NASA missions and other government, industry, and academic experimental testing needs for decades to come.

Acknowledgments

Although there are far too many to name individually, the authors would like to acknowledge the government and contractor teams who have contributed, and continue to contribute, to the conceptualization, advocacy, design, and construction of the Flight Dynamics Research Facility. With respect to the government team, the efforts of current and former members of the Langley Flight Dynamics Branch, Research Directorate, Center Operations Directorate, Jacobs Engineering, and the General Services Administration have made invaluable contributions to this multi-decade effort through requirements development and numerous detailed review cycles.

References

[1] Wenzinger, C. J., and Harris, T. A., "The Vertical Wind Tunnel of the National Advisory Committee For Aeronautics," NACA Report 387, 1931.

[2] Zimmerman, C. H., "Preliminary Tests in the N.A.C.A. Free-Spinning Wind Tunnel," NACA Report 557, 1936.

[3] Campbell, J. P., "Free and Semi-Free Model Flight-Testing Techniques Used in Low-Speed Studies of Dynamic Stability and Control," AGARDograph 76, Oct. 1963.

[4] Wolowicz, C. H., Bowman, J. S., and Gilbert, W. P., "Similitude Requirements and Scaling Relationships as Applied to Model Testing," NASA TP-1435, Aug. 1979.

[5] Chambers, J. R., "Cave of the Winds: The Remarkable History of the Langley Full-Scale Wind Tunnel," NASA SP-2014-614, 2014.

[6] Mangum, C. H., Harris, C. E., Allen, C. L., Craft, S., Hope, D. J., Kegelman, J. T., Mastaler, M. D., and Weiser, E. S., "LaRC 20-Year Center Revitalization Plan," NASA TM-2012-217592, Jul. 2012.

[7] Foster, J. V., Miller, L. J., Busan, R. C., Langston, S., and Hartman, D., "Recent NASA Wind Tunnel Free-Flight Testing Of A Multirotor Unmanned Aircraft System," *AIAA SciTech 2020 Forum*, AIAA Paper 2020-1504, Jan. 2020. https://doi.org/10.2514/6.2020-1504.

[8] Vicroy, D. D., "A Guide to Forced Oscillation Data Processing and Analysis," NASA TP–20210023569, Jun. 2023.

[9] Owens, D. B., Brandon, J. M., Croom, M. A., Fremaux, C. M., Heim, E. H., and Vicroy, D. D., "Overview of Dynamic Test Techniques for Flight Dynamics Research at NASA LaRC," *25th AIAA Aerodynamic Measurement Technology and Ground Testing Conference*, AIAA Paper 2006-3146, Jun. 2006. https://doi.org/10.2514/6.2006-3146.

[10] Cook, M., "On the Use of Small Scale Aircraft Models for Dynamic Wind Tunnel Investigation of Stability and Control," *Transactions of the Institute of Measurement and Control*, Vol. 9, No. 4, 1987, pp. 190–197. https://doi.org/10.1177/014233128700900405.

[11] Papageorgiou, G., and Glover, K., "Two-Degree-of-Freedom Control of an Actively Controlled Wind-Tunnel Model," *Journal of Guidance, Control, and Dynamics*, Vol. 25, No. 3, 2002, pp. 510–516. https://doi.org/10.2514/2.4911.

[12] Gatto, A., and Lowenberg, M. H., "Evaluation of a Three Degree of Freedom Test Rig for Stability Derivative Estimation," *Journal of Aircraft*, Vol. 43, No. 6, 2006, pp. 1747–1761. https://doi.org/10.2514/1.19821.

[13] Carnduff, S. D., Erbsloeh, S. D., Cooke, A. K., and Cook, M. V., "Characterizing Stability and Control of Subscale Aircraft from Wind-Tunnel Dynamic Motion," *Journal of Aircraft*, Vol. 46, No. 1, 2009, pp. 137–147. https://doi.org/10.2514/1.36730.

[14] Pattinson, J., Lowenberg, M. H., and Goman, M. G., "Multi-Degree-of-Freedom Wind-Tunnel Maneuver Rig for Dynamic Simulation and Aerodynamic Model Identification," *Journal of Aircraft*, Vol. 50, No. 2, 2013, pp. 551–566. https://doi.org/10.2514/1.C031924.

[15] Navaratna, P. D. B., Lowenberg, M. H., Neild, S. A., and Goman, M., "Self-Induced Roll–Yaw Oscillations of an Aircraft Model in a Wind Tunnel," *Journal of Aircraft*, Vol. 59, No. 1, 2022, pp. 3–14. https://doi.org/10.2514/1.C036157.

[16] Morelli, E. A., and Klein, V., *Aircraft System Identification: Theory and Practice*, 2nd ed., Sunflyte Enterprises, Williamsburg, VA, 2016.

[17] Simmons, B. M., Ackerman, K. A., and Asper, G. D., "Aero-Propulsive Damping Characterization for eVTOL Aircraft Using Free Motion Wind-Tunnel Testing," *AIAA SciTech 2025 Forum*, Jan. 2025. To be published.

[18] Vassberg, J., Dehaan, M., Rivers, M., and Wahls, R., "Development of a Common Research Model for Applied CFD Validation Studies," *26th AIAA Applied Aerodynamics Conference*, AIAA Paper 2008-6919, Aug. 2008. https://doi.org/10.2514/6.2008-6919.

[19] Rivers, M. B., and Dittberner, A., "Experimental Investigations of the NASA Common Research Model," *Journal of Aircraft*, Vol. 51, No. 4, 2014, pp. 1183–1193. https://doi.org/10.2514/1.C032626.

[20] Ueno, M., Kohzai, M., Koga, S., Kato, H., Nakakita, K., and Sudani, N., "80% Scaled NASA Common Research Model Wind Tunnel Test of JAXA at Relatively Low Reynolds Number," *51st AIAA Aerospace Sciences Meeting including the New Horizons Forum and Aerospace Exposition*, AIAA Paper 2013-493, Jan. 2013. https://doi.org/10.2514/6.2013-493.

[21] Uchiyama, T., Kohzai, M., Miki, H., Hirotani, T., Sudani, N., and Shutoku, H., "Experimental Investigation of a 160% Scaled NASA Common Research Model at Low Speed Conditions," *AIAA SciTech 2019 Forum*, AIAA Paper 2019-2190, Jan. 2019. https://doi.org/10.2514/6.2019-2190.

[22] Rivers, M. B., "NASA Common Research Model: A History and Future Plans," *AIAA Aviation 2019 Forum*, AIAA Paper 2019-3725, Jun. 2019. https://doi.org/10.2514/6.2019-3725.

[23] Cartieri, A., Hue, D., Chanzy, Q., and Atinault, O., "Experimental Investigations on the Common Research Model at ONERA-S1MA – Comparison with DPW Numerical Results," *55th AIAA Aerospace Sciences Meeting*, AIAA Paper 2017-0964, Jan. 2017. https://doi.org/10.2514/6.2017-0964.

[24] Waldmann, A., Lutz, T., and Krämer, E., "Wind Tunnel Support System Influence on NASA Common Research Model at Low-Speed Conditions," *Journal of Aircraft*, Vol. 55, No. 5, 2018, pp. 1762–1772. https://doi.org/10.2514/1.C034440.

[25] Cartieri, A., "Experimental Investigations on the Common Research Model at ONERA-S2MA," *AIAA Scitech 2020 Forum*, AIAA Paper 2020-0779, Jan. 2020. https://doi.org/10.2514/6.2020-0779.

[26] Beyers, M. E., and Moulton, B. E., "Stability Derivatives Due to Oscillations in Roll for the Standard Dynamics Model at Mach 0.6," LTR-UA-64, National Research Council Canada, National Aeronautical Establishment, 1983.

[27] Cyran, F. B., "Sting Interference Effects on the Static Dynamic, and Base Pressure Measurements of the Standard Dynamics Model Aircraft at Mach Numbers 0.3 through 1.3," AEDC TR-81-3, Arnold Engineering Development Center, Aug. 1981.

[28] Coulter, S., and Marquart, E., "Cross and Cross-Coupling Derivative Measurements on the Standard Dynamics Model at AEDC," *12th Aerodynamic Testing Conference*, AIAA Paper 1982-596, Mar. 1982. https://doi.org/10.2514/6.1982-596.

[29] Winchenbach, G., Chelekis, R., Uselton, B., and Hathaway, W., "Comparison of Free-Flight and Wind Tunnel Data for a Generic Fighter Configuration," *9th Atmospheric Flight Mechanics Conference*, AIAA Paper 1982-1365, Aug. 1982. https://doi.org/10.2514/6.1982-1365.

[30] Uselton, B., and Haberman, D., "Summary of Sting Interference Effects for Cone, Missile, and Aircraft Configurations as Determined by Dynamic and Static Measurements," *9th Atmospheric Flight Mechanics Conference*, AIAA Paper 1982-1366, Aug. 1982. https://doi.org/10.2514/6.1982-1366.

[31] Beyers, M., "Subsonic Roll Oscillation Experiments on the Standard Dynamics Model," *10th Atmospheric Flight Mechanics Conference*, AIAA Paper 1983-2134, Aug. 1983. https://doi.org/10.2514/6.1983-2134.

[32] Beyers, M. E., Kapoor, K. B., and Moulton, B. E., "Pitch-and Yaw-Oscillation Experiments on the Standard Dynamics Model at Mach 0.6," LTR-UA-76, National Research Council Canada, National Aeronautical Establishment, 1984.

[33] Winchenbach, G., Uselton, R. L., Hathaway, W. H., and Chelekis, R. M., "Free-Flight and Wind-Tunnel Data for a Generic Fighter Configuration," *Journal of Aircraft*, Vol. 21, No. 1, 1984, pp. 5–13. https://doi.org/10.2514/3.48215.

[34] Jansson, T., and Torngren, L., "New Dynamic Testing Techniques and Related Results at FFA," AGARD CP-386, Nov. 1985.

[35] Jermey, C., and Schiff, L., "Wind-Tunnel Investigation of the Aerodynamic Characteristics of the Standard Dynamics Model in Coning Motion at Mach 0.6," *12th Atmospheric Flight Mechanics Conference*, AIAA Paper 1985-1828, Aug. 1985. https://doi.org/10.2514/6.1985-1828.

[36] Jermey, C., and Schiff, L. B., "Aerodynamic Characteristics of the Standard Dynamics Model in Coning Motion at Mach 0.6," NASA TM-86717, Jul. 1985.

[37] Balakrishna, S., and Niranjana, T., "Wind Tunnel Dynamic Flying Study of the Pitching Moment Derivatives of the Standard Dynamics Model in Active Control," *14th Atmospheric Flight Mechanics Conference*, AIAA Paper 1987-2626, Aug. 1987. https://doi.org/10.2514/6.1987-2626.

[38] Guglieri, G., and Quagliotti, F., "Determination of Dynamic Stability Parameters in a Low Speed Wind Tunnel," *9th Applied Aerodynamics Conference*, AIAA Paper 1991-3245, Sep. 1991. https://doi.org/10.2514/6.1991-3245.

[39] Guglieri, G., and Quagliotti, F. B., "Dynamic Stability Derivatives Evaluation in a Low-Speed Wind Tunnel," *Journal of Aircraft*, Vol. 30, No. 3, 1993, pp. 421–423. https://doi.org/10.2514/3.46357.

[40] Ueno, M., and Miwa, H., "New Dynamic Stability Equipment for Transonic Wind Tunnel Testing at NAL," *39th Aerospace Sciences Meeting and Exhibit*, AIAA Paper 2001-406, Jan. 2001. https://doi.org/10.2514/6.2001-406.

[41] Erm, L. P., and Ol, M., "An Assessment of the Usefulness of Water Tunnels for Aerodynamic Investigations," DSTO TR-2803, Defence Science and Technology Organisation, Dec. 2012.

[42] Erm, L. P., "An Experimental Investigation Into the Feasibility of Measuring Static and Dynamic Aerodynamic Derivatives in the DSTO Water Tunnel," DSTO TR-2600, Defence Science and Technology Organisation, Aug. 2013.

[43] Montgomery, D. C., *Design And Analysis of Experiments*, 9th ed., John Wiley & Sons, Inc., Hoboken, NJ, 2017.

[44] Myers, R. H., Montgomery, D. C., and Anderson-Cook, C. M., *Response Surface Methodology: Process and Product Optimization Using Designed Experiments*, 4th ed., John Wiley & Sons, Hoboken, NJ, 2016.

[45] Simmons, B. M., "Evaluation of Response Surface Experiment Designs for Distributed Propulsion Aircraft Aero-Propulsive Modeling," *AIAA SciTech 2023 Forum*, AIAA Paper 2023-2251, Jan. 2023. https://doi.org/10.2514/6.2023-2251.

[46] DeLoach, R., "Applications of Modern Experiment Design to Wind Tunnel Testing at NASA Langley Research Center," *36th AIAA Aerospace Sciences Meeting and Exhibit*, AIAA Paper 1998-0713, Jan. 1998. https://doi.org/10.2514/6.1998-713.

[47] Morelli, E. A., and DeLoach, R., "Wind Tunnel Database Development Using Modern Experiment Design and Multivariate Orthogonal Functions," *41st Aerospace Sciences Meeting and Exhibit*, AIAA Paper 2003-653, Jan. 2003. https://doi.org/10.2514/6.2003-653.

[48] Busan, R. C., Rothhaar, P. M., Croom, M. A., Murphy, P. C., Grafton, S. B., and O'Neal, A. W., "Enabling Advanced Wind-Tunnel Research Methods Using the NASA Langley 12-Foot Low-Speed Tunnel," *14th AIAA Aviation Technology, Integration, and Operations Conference*, AIAA Paper 2014-3000, Jun. 2014. https://doi.org/10.2514/6.2014-3000.

[49] Murphy, P. C., and Landman, D., "Experiment Design for Complex VTOL Aircraft with Distributed Propulsion and Tilt Wing," *AIAA Atmospheric Flight Mechanics Conference*, AIAA Paper 2015-0017, Jan. 2015. https://doi.org/10.2514/6.2015-0017.

[50] Murphy, P. C., Hatke, D., Aubuchon, V. V., Weinstein, R., and Busan, R. C., "Preliminary Steps in Developing Rapid Aero Modeling Technology," *AIAA SciTech 2020 Forum*, AIAA Paper 2020-0764, Jan. 2020. https://doi.org/10.2514/6.2020-0764.

[51] Busan, R. C., Murphy, P. C., Hatke, D. B., and Simmons, B. M., "Wind Tunnel Testing Techniques for a Tandem Tilt-Wing, Distributed Electric Propulsion VTOL Aircraft," *AIAA SciTech 2021 Forum*, AIAA Paper 2021-1189, Jan. 2021. https://doi.org/10.2514/6.2021-1189.

[52] Simmons, B. M., and Murphy, P. C., "Aero-Propulsive Modeling for Tilt-Wing, Distributed Propulsion Aircraft Using Wind Tunnel Data," *Journal of Aircraft*, Vol. 59, No. 5, 2022, pp. 1162–1178. https://doi.org/10.2514/1.C036351.

[53] Simmons, B. M., "Efficient Variable-Pitch Propeller Aerodynamic Model Development for Vectored-Thrust eVTOL Aircraft," *AIAA AVIATION 2022 Forum*, AIAA Paper 2022-3817, Jun. 2022. https://doi.org/10.2514/6.2022-3817.

[54] Simmons, B. M., and Busan, R. C., "Statistical Wind-Tunnel Experimentation Advancements for eVTOL Aircraft Aero-Propulsive Model Development," *AIAA SciTech 2024 Forum*, AIAA Paper 2024-2482, Jan. 2024. https://doi.org/10.2514/6.2024-2482.

[55] Weinstein, R., and Simmons, B. M., "Experimental Characterization of an Electric Ducted Fan for the SUSAN 25% Scale Research Vehicle," *AIAA SciTech 2024 Forum*, AIAA Paper 2024-1524, Jan. 2024. https://doi.org/10.2514/6.2024-1524.

[56] Morelli, E. A., "Multiple Input Design for Real-Time Parameter Estimation in the Frequency Domain," *13th IFAC Conference on System Identification*, Aug. 2003. https://doi.org/10.1016/S1474-6670(17)34833-4.

[57] Morelli, E. A., "Flight-Test Experiment Design for Characterizing Stability and Control of Hypersonic Vehicles," *Journal of Guidance, Control, and Dynamics*, Vol. 32, No. 3, 2009, pp. 949–959. https://doi.org/10.2514/1.37092.

[58] Morelli, E. A., "Practical Aspects of Multiple-Input Design for Aircraft System Identification Flight Tests," *AIAA AVIATION 2021 Forum*, AIAA Paper 2021-2795, Aug. 2021. https://doi.org/10.2514/6.2021-2795.

[59] Morelli, E. A., and Grauer, J. A., "Advances in Aircraft System Identification at NASA Langley Research Center," *Journal of Aircraft*, Vol. 60, No. 5, 2023, pp. 1354–1370. https://doi.org/10.2514/1.C037274.

[60] Murphy, P. C., and Brandon, J., "Efficient Testing Combining Design of Experiment and Learn-to-Fly Strategies," *AIAA Atmospheric Flight Mechanics Conference*, AIAA Paper 2017-0696, Jan. 2017. https://doi.org/10.2514/6.2017-0696.

[61] Simmons, B. M., Morelli, E. A., Busan, R. C., Hatke, D. B., and O'Neal, A. W., "Aero-Propulsive Modeling for eVTOL Aircraft Using Wind Tunnel Testing with Multisine Inputs," *AIAA AVIATION 2022 Forum*, AIAA Paper 2022-3603, Jun. 2022. https://doi.org/10.2514/6.2022-3603.

[62] Klein, V., Batterson, J. G., and Murphy, P. C., "Determination of Airplane Model Structure from Flight Data by Using Modified Stepwise Regression," NASA TP-1916, Oct. 1981.

[63] Morelli, E. A., and Grauer, J. A., "Practical Aspects of Frequency-Domain Approaches for Aircraft System Identification," *Journal of Aircraft*, Vol. 57, No. 2, 2020, pp. 268–291. https://doi.org/10.2514/1.C035599.